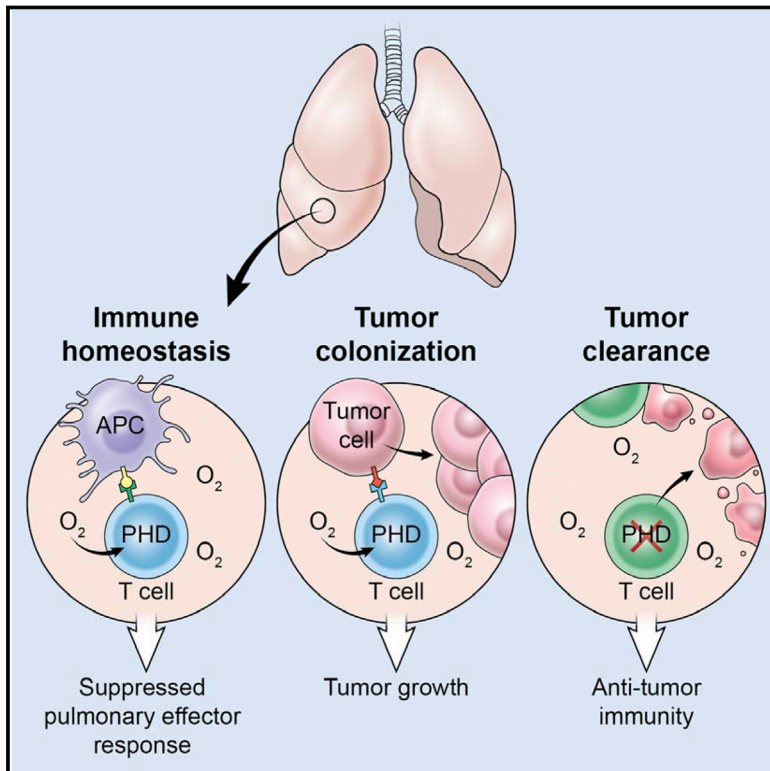# Cell

Oxygen Sensing by T Cells Establishes an Immunologically Tolerant Metastatic Niche

Graphical Abstract

Authors
David Clever, Rahul Roychoudhuri, Michael G. Constantinides, ..., Ananda W. Goldrath, Yasmine Belkaid, Nicholas P. Restifo

Correspondence
david.clever@osumc.edu (D.C.), restifo@nih.gov (N.P.R.)

In Brief

PHD-protein-mediated oxygen sensing by T cells creates an immunoenvironment in the lung that facilitates the establishment of cancer metastasis.

Highlights

- PHD proteins function redundantly as oxygen sensors in T cells

- T-cell-intrinsic expression of PHD proteins maintains immune tolerance in the lung

- PHD proteins support cancer metastasis to the lung

- Blockade of T-cell-intrinsic PHD proteins promotes anti-tumor immunity

Data Resources

GSE85131

CrossMark

CellPress

Oxygen Sensing by T Cells Establishes an Immunologically Tolerant Metastatic Niche

David Clever,[1,2,*] Rahul Roychoudhuri,[1,3] Michael G. Constantinides,[4] Michael H. Askenase,[4] Madhusudhanan Sukumar,[1] Christopher A. Klebanoff,[1,6] Robert L. Eil,[1] Heather D. Hickman,[7] Zhiya Yu,[1] Jenny H. Pan,[1] Douglas C. Palmer,[1] Anthony T. Phan,[8] John Goulding,[8] Luca Gattinoni,[9] Ananda W. Goldrath,[8] Yasmine Belkaid,[4,5] and Nicholas P. Restifo[1,10,11,*]

[1]Surgery Branch, National Cancer Institute (NCI), National Institutes of Health (NIH), Bethesda, MD 20892, USA
[2]Medical Scientist Training Program, The Ohio State University College of Medicine, Columbus, OH 43210, USA
[3]Laboratory of Lymphocyte Signaling and Development, Babraham Institute, Cambridge CB22 3AT, UK
[4]Mucosal Immunology Section, Laboratory of Parasitic Diseases, National Institute of Allergy and Infectious Diseases (NIAID), NIH, Bethesda, MD 20892, USA
[5]NIAID Microbiome Program Initiative, NIAID/NIH, Bethesda, MD 20892, USA
[6]Center for Cell Engineering and Department of Medicine, Memorial Sloan Kettering Cancer Center, New York, NY 10065, USA
[7]Laboratory of Viral Diseases, NIAID, NIH, Bethesda, MD 20892, USA
[8]Division of Biological Sciences, University of California, San Diego, La Jolla, CA 92093, USA
[9]Experimental Transplantation Immunology Branch, NCI, NIH, Bethesda, MD 20892, USA
[10]Center for Cell-based Therapy, National Cancer Institute, National Institutes of Health (NIH), Bethesda, MD 20892, USA
[11]Lead Contact
*Correspondence: david.clever@osumc.edu (D.C.), restifo@nih.gov (N.P.R.)
http://dx.doi.org/10.1016/j.cell.2016.07.032

SUMMARY

Cancer cells must evade immune responses at distant sites to establish metastases. The lung is a frequent site for metastasis. We hypothesized that lung-specific immunoregulatory mechanisms create an immunologically permissive environment for tumor colonization. We found that T-cell-intrinsic expression of the oxygen-sensing prolyl-hydroxylase (PHD) proteins is required to maintain local tolerance against innocuous antigens in the lung but powerfully licenses colonization by circulating tumor cells. PHD proteins limit pulmonary type helper (Th)-1 responses, promote CD4$^+$-regulatory T (T$_{reg}$) cell induction, and restrain CD8$^+$ T cell effector function. Tumor colonization is accompanied by PHD-protein-dependent induction of pulmonary T$_{reg}$ cells and suppression of IFN-γ-dependent tumor clearance. T-cell-intrinsic deletion or pharmacological inhibition of PHD proteins limits tumor colonization of the lung and improves the efficacy of adoptive cell transfer immunotherapy. Collectively, PHD proteins function in T cells to coordinate distinct immunoregulatory programs within the lung that are permissive to cancer metastasis.

INTRODUCTION

Metastasis is the cause of more than 90% of cancer deaths and is a major obstacle for curative therapy (Valastyan and Weinberg, 2011). Metastatic dissemination involves a complex interaction between circulating tumor cells and the site of secondary coloni-zation. Local immunity is an important feature of metastatic sites, and circulating tumor cells must evade local immune responses for successful metastasis (Massagué and Obenauf, 2016). The lung is a common metastatic site for numerous cancer types including malignant melanoma (Minn et al., 2005). The extensive capillary network perfusing the lung parenchyma provides an anatomical mechanism for dissemination to this site. We hypothesized that the lungs also form an immunologically favorable site for cancer metastasis.

T cells play a critical role in coordinating immune function. Whereas effector T (T$_{eff}$) cells promote immune activation and can drive clearance of infections and cancer, regulatory T (T$_{reg}$) cells, dependent upon the transcription factor Foxp3, suppress their function, preventing excessive autoimmune and allergic reactions (Gavin et al., 2007; Sakaguchi et al., 1985). Inflammatory T$_{eff}$ cell responses are restrained in the lung despite continuous exposure to innocuous foreign antigens (Holt et al., 2008). While many specialized cell types are important regulators of pulmonary tolerance (de Heer et al., 2004; Stumbles et al., 1998), T-cell-intrinsic molecular programs may also influence site-specific immunity in the lung.

The prolyl hydroxylase domain containing family of proteins, comprising PHD1, PHD2, and PHD3, function as intracellular sensors of oxygen (Bruick and McKnight, 2001; Epstein et al., 2001). PHD enzymes are Fe^{2+}-dependent dioxygenases that use a conserved two-histidine, one-carboxylate motif to coordinate Fe^{2+}, 2-oxoglutarate, and free oxygen at the active site (Kaelin and Ratcliffe, 2008). In well-oxygenated environments the PHD enzymes catalyze post-translational hydroxylation of substrate proteins, including hypoxia-inducible factors HIF1α and HIF2α (collectively HIFα), which are then degraded (Jaakkola et al., 2001). In T cells HIFα can drive effector responses by promoting differentiation of CD4$^+$ Th17 cells (Dang et al., 2011; Shi et al., 2011), CD8$^+$ T cell effector function (Doedens et al., 2013),

and interferon (IFN)-γ production within T regulatory cells (Lee et al., 2015). This led us to hypothesize that the oxygen-sensing PHD proteins might influence T cell differentiation and function, particularly in the oxygen-rich environment of the lung.

Here, we show that T-cell-intrinsic expression of the PHD proteins suppresses pulmonary inflammation against innocuous foreign antigens but powerfully licenses tumor colonization of the lung. Upon tumor colonization PHD proteins promote T_{reg} cell expansion and restrain IFN-γ-dependent clearance of tumors. Importantly, genetic and pharmacological disruption of PHD proteins limits tumor colonization of the lung and improves the efficacy of T-cell-based adoptive cell therapy (ACT). These results indicate that T-cell-intrinsic expression of the oxygen-sensing PHD proteins coordinates a tissue-specific immunoregulatory program that suppresses mild inflammatory pathology but readily permits cancer metastasis in the lung.

RESULTS

PHD Proteins Function within T Cells to Limit Pulmonary Effector Responses

Pulmonary tolerance requires suppression of inflammatory T cell responses under physiologic conditions. We asked whether T-cell-intrinsic expression of the oxygen-sensing PHD proteins contributes to site-specific tolerance in the lung. We generated mice harboring a T-cell-specific deletion of all three PHD proteins (henceforth PHD-tKO). *Cd4*-driven Cre recombinase expression resulted in significant reduction of *Egln1*, *Egln2*, and *Egln3* mRNA transcripts, which encode PHD2, PHD1, and PHD3 proteins respectively, in CD4$^+$, CD8$^+$, and NKT T cells, but not in other lymphoid cell subsets (Figure S1A). Upon gross evaluation, we observed a patchy hemorrhagic appearance within the lungs of PHD-tKO mice that was not present among wild-type (WT) littermates (Figure 1A). Histologic examination revealed the presence of diffuse alveolar hemorrhage (DAH) of variable severity in PHD-tKO mice (Figures 1B and 1C). PHD-tKO mice had increased serum autoantibodies, which can be elevated upon immune-mediated tissue damage (Figure S1B). Pathology in PHD-tKO mice was only observed in the lung, and we did not detect abnormal liver and pancreas enzymes in the blood (Figure 1D).

PHD-tKO animals showed no defects in thymocyte number or phenotypic distribution (Figure S1C). Similar numbers of CD4$^+$ and CD8$^+$ T lymphocytes were detected in peripheral blood and secondary lymphoid organs (Figure S1D). In the bone marrow of PHD-tKO mice, there was a slight reduction in CD8$^+$ T cells but similar numbers of CD4$^+$ T cells (Figure S1D). As the bone marrow is a reservoir of memory T cells, we evaluated the differentiation state of T cells in WT and PHD-tKO mice. There was a similar distribution of naive and effector CD4$^+$ T cells in WT and PHD-tKO mice (Figure S1E). However, increased frequencies of terminally differentiated CD8$^+$ T cells were observed in the peripheral blood, spleen, and bone marrow of PHD-tKO mice (Figures S1E and S1F). This might explain the reduction of CD8$^+$ T cells in the bone marrow of PHD-tKO mice and suggests a role for the PHD proteins in restraining terminal CD8$^+$ T cell differentiation.
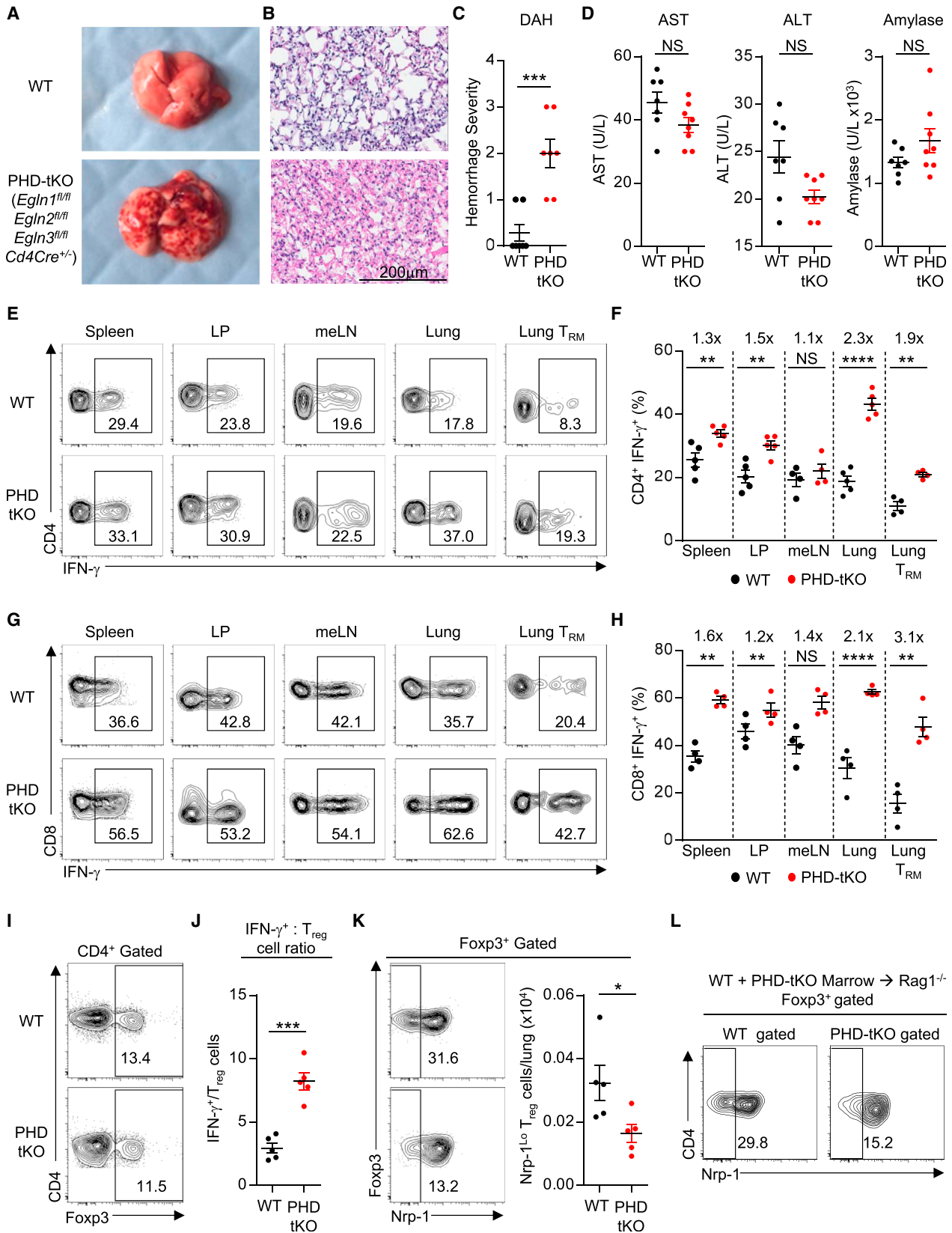
T cells can drive immunopathology in the lung. We observed increased numbers of pulmonary CD4$^+$ and CD8$^+$ T cells in PHD-tKO mice (Figure S1G). Additionally, pulmonary T cells in PHD-tKO mice had increased expression of the activation markers CD44 (Figure S1H), CD25, CTLA-4, and GITR (Figure S1I). Importantly, in PHD-tKO mice we measured increased expression of IFN-γ by CD4$^+$ and CD8$^+$ T cells isolated from multiple lymphoid and non-lymphoid organs, yet this was most pronounced in the lung (Figures 1E–1H and S1G). Elevated IFN-γ production was more significant in the lung, including among pulmonary tissue resident memory (T_{RM}) T cells, than in T cells residing in mediastinal lymph nodes (meLN) (Figures 1F and 1H). These data suggest that the PHD proteins predominantly restrain T cell effector function in the lung parenchyma and airway-associated lymphoid tissue. We also measured increased expression of cytolytic effector molecules in pulmonary CD4$^+$ and CD8$^+$ T cells in PHD-tKO mice (Figure S1J). Additionally, we observed increased expression of IFN-γ, but not other effector cytokines, in pulmonary NKT cells from PHD-tKO mice (Figure S1K). Thus, T-cell-intrinsic expression of PHD proteins limits effector T cell function and prevents mild spontaneous immune pathology in the lung.

PHD Proteins Maintain Pulmonary Nrp-1^{Lo} T_{reg} Cells

T_{reg} cells suppress deleterious effector T cell responses directed against self and innocuous foreign antigens (Strickland et al., 2006). We asked whether increased effector function observed in pulmonary T cells from PHD-tKO mice is secondary to a local deficit in T_{reg} cells. Pulmonary T_{reg} cell frequency and absolute number was similar in PHD-tKO mice compared to WT controls (Figures 1I and S1G). The overall phenotypic profile thus revealed a significantly elevated IFN-γ^+ T_{eff} to T_{reg} cell ratio in lungs of PHD-tKO mice (Figure 1J).

The stability of Foxp3$^+$ T_{reg} cells is an important parameter in their immunoregulatory function. T_{reg} cell stability is proportional to the level of demethylation within the T_{reg}-specific-demethylated region (TSDR) of the *Foxp3* locus (Floess et al., 2007). TSDR CpG methylation was similar in WT and PHD-tKO T_{reg} cells (Figure S1L). Consistently, the stability of Foxp3 expression was similar in WT and PHD-tKO T_{reg} cells following restimulation in vitro or upon in vivo transfer into Rag1$^{-/-}$ hosts (Figures S1M–S1O).

T_{reg} cell populations are comprised of thymically derived T_{reg} (tT_{reg}) cells and peripherally induced iT_{reg} cells (Bluestone and Abbas, 2003). iT_{reg} cells are particularly important in suppressing effector T cell responses at mucosal sites (Josefowicz et al., 2012). Neuropilin-1 (Nrp-1) has been proposed as a marker to distinguish tT_{reg} cells from iT_{reg} cells (Weiss et al., 2012; Yadav et al., 2012). We detected a reduction in the frequency and number of Nrp-1^{Lo} T_{reg} cells in the lungs of PHD-tKO mice (Figure 1K). Nrp-1 expression can be induced on T_{reg} cells in inflammatory environments (Weiss et al., 2012). This raised the possibility that the observed reduction in pulmonary Nrp-1^{Lo} T_{reg} cells in PHD-tKO mice is the result of induced Nrp-1 expression in the inflamed lung environment. To exclude this possibility, we tested whether differences in Nrp-1 expression between WT and PHD-tKO T_{reg} cells exist when cells are exposed to an identical pulmonary environment. We reconstituted lethally ablated Rag1$^{-/-}$

A

WT

PHD-tKO
(*Egln1^{fl/fl}*
Egln2^{fl/fl}
Egln3^{fl/fl}
Cd4Cre^{+/-})

B

200μm

C

DAH

D

AST — NS

ALT — NS

Amylase — NS

E

Spleen, LP, meLN, Lung, Lung T_{RM}

WT

29.4, 23.8, 19.6, 17.8, 8.3

PHD tKO

33.1, 30.9, 22.5, 37.0, 19.3

CD4 / IFN-γ

F

1.3x ** | 1.5x ** | 1.1x NS | 2.3x **** | 1.9x **

CD4^+ IFN-γ^+ (%)

Spleen, LP, meLN, Lung, Lung T_{RM}

● WT ● PHD-tKO

G

Spleen, LP, meLN, Lung, Lung T_{RM}

WT

36.6, 42.8, 42.1, 35.7, 20.4

PHD tKO

56.5, 53.2, 54.1, 62.6, 42.7

CD8 / IFN-γ

H

1.6x ** | 1.2x ** | 1.4x NS | 2.1x **** | 3.1x **

CD8^+ IFN-γ^+ (%)

Spleen, LP, meLN, Lung, Lung T_{RM}

● WT ● PHD-tKO

I

CD4^+ Gated

WT

13.4

PHD tKO

11.5

CD4 / Foxp3

J

IFN-γ^+ : T_{reg} cell ratio

IFN-γ^+/T_{reg} cells

***

WT PHD tKO

K

Foxp3^+ Gated

31.6

13.2

Foxp3 / Nrp-1

Nrp-1^{Lo} T_{reg} cells/lung (x10^4)

*

WT PHD tKO

L

WT + PHD-tKO Marrow → Rag1^{-/-}
Foxp3^+ gated

WT gated | PHD-tKO gated

29.8 | 15.2

CD4 / Nrp-1

(legend on next page)

mice with bone marrow isolated from congenically distinguishable WT or PHD-tKO mice in a 1:1 mixture and evaluated pulmonary T_{reg} cells following reconstitution. Importantly, we observed a reduced frequency of Nrp-1^{Lo} cells within PHD-tKO pulmonary T_{reg} cells (Figure 1L). Thus, the reduced frequency of Nrp-1^{Lo} T_{reg} cells in lungs of PHD-tKO mice is not secondary to the inflamed environment but instead is a cell-intrinsic phenomenon.

PHD Proteins Restrain Th1 Inflammation against Innocuous Foreign Antigens

Respiratory surfaces are chronically exposed to immunogenic and normally non-pathogenic environmental antigens. These stimuli predominantly induce non-inflammatory immunosuppressive T_{reg} cell responses or Th2 responses, which in certain instances can lead to the development of asthma (Strickland et al., 2006; Stumbles et al., 1998). We hypothesized that the mild steady-state pathology observed in lungs of PHD-tKO mice was caused by excessive inflammatory responses against innocuous environmental antigens. To test this, we sensitized and challenged the airway of WT and PHD-tKO mice with house dust mite (HDM) extract.

HDM challenge promoted similar expansion of pulmonary CD4$^+$ T cells in WT and PHD-tKO mice (Figure S2A). HDM challenge induced a robust expansion of pulmonary Th2 cells in WT mice (Figures 2A and 2C) but failed to do so in PHD-tKO mice. Remarkably, we instead observed a dramatic increase in IFN-γ^+ Th1 cells in lungs of PHD-tKO mice upon HDM challenge (Figures 2A and 2C). Additionally, HDM challenge induced accumulation of pulmonary T_{reg} cells that was reduced in PHD-tKO mice compared to WT controls (Figures 2B and 2C). PHD-tKO mice also exhibited greater expansion of CD8$^+$ T cells and induction of IFN-γ expression among these cells upon HDM challenge (Figures 2D, 2E, and S2B). Consequently, PHD-tKO mice suffered from more severe inflammation following chronic HDM exposure that was consistent with Th1 rather than Th2-driven immunopathology including vasculitis and diffuse tissue damage leading to alveolar hemorrhage (Figures 2F–2H). Thus, the PHD proteins coordinate a T-cell-intrinsic program that restrains inflammatory T cell effector responses against innocuous foreign antigens in the lung.

PHD Proteins Regulate Reciprocal iT$_{reg}$ and Th1 Differentiation Programs

The decrease in steady-state pulmonary Nrp-1^{Lo} T_{reg} cells and reduction in HDM-induced T_{reg} cell accumulation suggested that the PHD proteins might promote iT$_{reg}$ cell differentiation. Stimulation of naive CD4$^+$ T cells in the presence of interleukin-2 (IL-2) and TGF-β promotes the development of iT$_{reg}$ cells in vitro and in vivo (Chen et al., 2003; Li et al., 2006). To determine whether PHD proteins are required for iT$_{reg}$ cell differentiation, we evaluated the gene expression profile of PHD-tKO and WT CD4$^+$ T cells primed in vitro in conditions favoring iT$_{reg}$ cell generation. RNA sequencing revealed widespread gene expression differences between PHD-tKO and WT cells (545 upregulated and 344 downregulated genes in PHD-tKO). Importantly, a significant reduction in *Foxp3* expression and induction of genes encoding the Th1 lineage specifying transcription factor T-bet (*Tbx21*) and effector cytokine IFN-γ (*Ifng*) was observed in PHD-tKO cells (Figure 3A). By contrast, genes encoding Th2 and Th17 lineage specifying transcription factors and effector cytokines were expressed at similar levels in WT and PHD-tKO cells (Figure 3A). Competitive antagonism of PHD protein enzymatic activity using a pan-PHD inhibitor, dimethyloxalylglycine (DMOG), caused similar changes in global gene expression as those observed in PHD-tKO T cells (Figures S3A and S3B).

To further evaluate the requirement for PHD proteins in iT$_{reg}$ cell differentiation, we stimulated naive CD4$^+$ T cells isolated from WT and PHD-tKO mice in the presence of titrated concentrations of TGF-β. PHD proteins were required for TGF-β-driven induction of Foxp3 and repression of T-bet (Figures 3B–3D). Consistently, higher amounts of IFN-γ were detected in supernatants collected from PHD-tKO cell cultures (Figure 3E). Naive PHD-tKO CD4$^+$ T cells also demonstrated impaired iT$_{reg}$ conversion in vivo following transfer into Rag1$^{-/-}$ recipient animals (Figure S3C). These results indicate that PHD proteins regulate reciprocal iT$_{reg}$ and Th1 differentiation programs.

Foxp3$^+$ iT$_{reg}$ cells derived from PHD-tKO cells or WT cells stimulated in the presence of DMOG expressed high levels of T-bet (Figures 3B and 3F). T-bet expression can be induced in T_{reg} cells in response to IFN-γ (Koch et al., 2012). Indeed, blockade of IFN-γ limited T-bet expression in PHD-tKO Foxp3$^+$

Figure 1. PHD Proteins Function within T Cells to Suppress Spontaneous Pulmonary Inflammation

(A) Gross morphology of lungs from *Egln1$^{fl/fl}$ Egln2$^{fl/fl}$ Egln3$^{fl/fl}$ CD4Cre$^{+/-}$* triple-knockout (PHD-tKO) and Cre-negative wild-type (WT) littermate mice.

(B) H&E stains of WT and PHD-tKO lungs demonstrating diffuse alveolar hemorrhage (n = 7 mice per group).

(C) Histopathology scoring of lung tissue from WT and PHD-tKO mice (n = 7 mice per group).

(D) Titers of hepatic AST and ALT and pancreatic amylase in the sera of WT and PHD-tKO mice.

(E and F) IFN-γ production by CD4$^+$ T cells from spleen, small intestine lamina propria (LP), mediastinal lymph node (meLN), lung, and pulmonary tissue resident memory (T_{RM}) cells in WT and PHD-tKO mice. Representative flow cytometry (E) and replicate values (F) are shown. Fold increase in frequency of CD4$^+$ IFN-γ^+ T cells in PHD-tKO mice normalized to WT is provided for each organ.

(G and H) IFN-γ production by CD8$^+$ T cells in the indicated organs in WT and PHD-tKO mice. Representative flow cytometry (G) and replicate values (H) are shown. Fold increase in frequency of CD8$^+$ IFN-γ^+ T cells in PHD-tKO mice normalized to WT is provided for each organ.

(I) Frequency of pulmonary Foxp3$^+$ T_{reg} cells in WT and PHD-tKO mice.

(J) Ratio of total numbers of CD4$^+$ and CD8$^+$ IFN-γ^+ T_{eff} cells to Foxp3$^+$ T_{reg} cells in the lungs of WT and PHD-tKO mice.

(K) Distribution of Nrp-1 -Hi and -Lo populations among pulmonary Foxp3$^+$ T_{reg} cells in WT and PHD-tKO mice. Representative flow cytometry and absolute numbers of Nrp-1^{Lo} T_{reg} cells are shown.

(L) Representative flow cytometry of Nrp-1 expression by WT and PHD-tKO pulmonary Foxp3$^+$ T_{reg} cells from WT and PHD-tKO mixed bone marrow chimeric mice.

Data are representative of two or more independent experiments with three or more mice per genotype. Mice were analyzed at 3 months of age unless otherwise specified. Bars and error represent mean ± SEM of replicate measurements. *p < 0.05, **p < 0.01, ***p < 0.001, ****p < 0.0001 (Student's t test).
See also Figure S1.
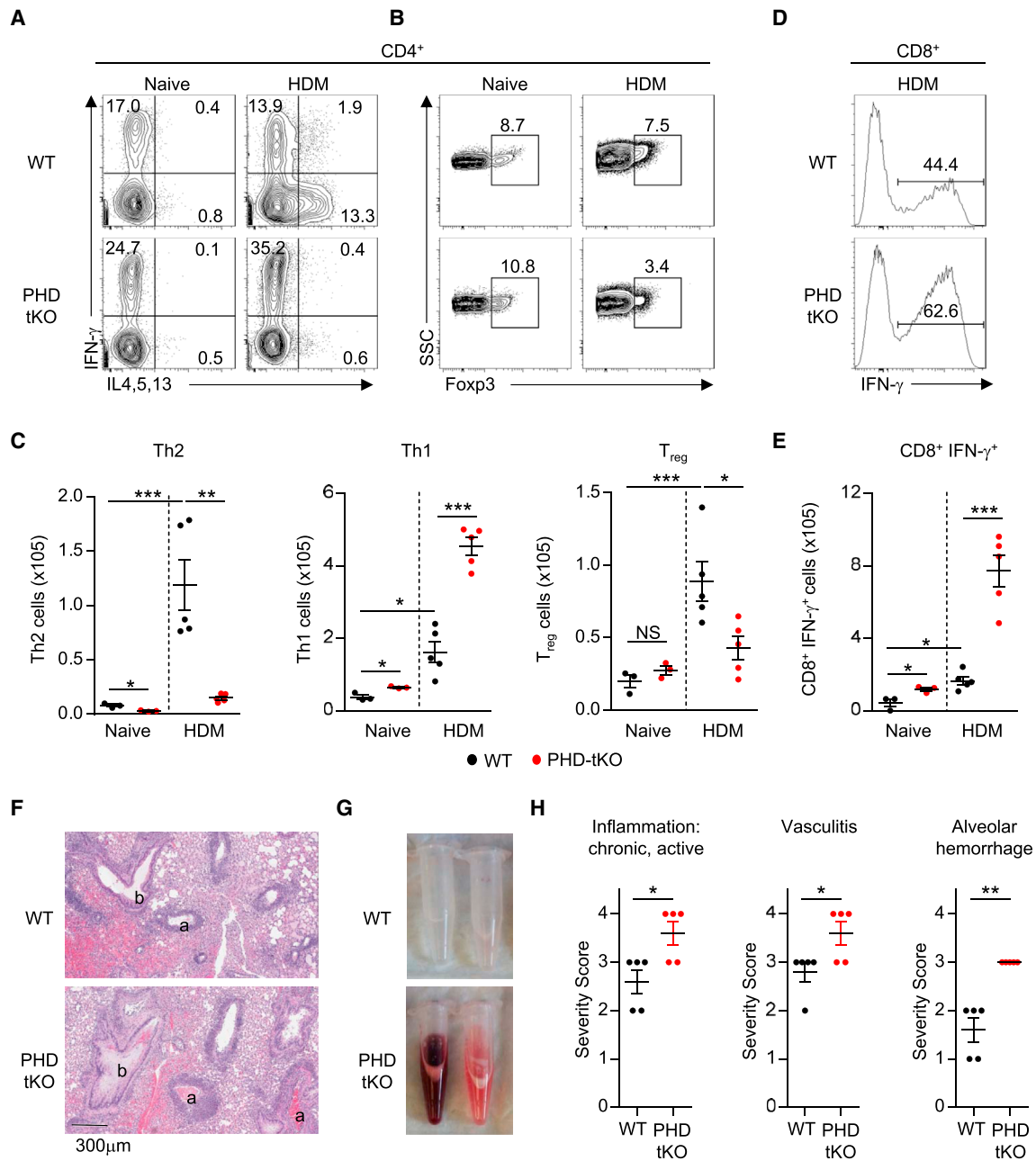
Figure 2. T-Cell-Intrinsic PHD Proteins Restrain Th1 Inflammation against Innocuous Antigens

(A and B) Flow cytometry analysis of Th1 and Th2 cytokine production (A) and Foxp3 expression (B) by pulmonary CD4$^+$ T cells from naive and house dust mite (HDM)-challenged WT and PHD-tKO mice.

(C) Total numbers of pulmonary Th2, Th1, and T$_{reg}$ cells in naive and HDM-challenged WT and PHD-tKO mice.

(D and E) IFN-γ production by pulmonary CD8$^+$ T cells from HDM-challenged WT and PHD-tKO mice. Representative flow cytometry (D) and total numbers of CD8$^+$ IFN-γ^+ T cells (E) are shown.

(F) Representative H&E stains of WT and PHD-tKO lungs following airway sensitization and challenge with house dust mite extract. a, arteriole; b, bronchiole.

(G) Representative bronchoalveolar lavage fluid appearance from WT and PHD-tKO mice.

(H) Histopathology scoring of lung tissue from HDM-challenged WT and PHD-tKO mice

Data are representative of two or more independent experiments with three or more mice per group. Bars and error represent mean ± SEM of replicate measurements. *$p < 0.05$, **$p < 0.01$, ***$p < 0.001$, ****$p < 0.0001$ (Student's t test).

See also Figure S2.
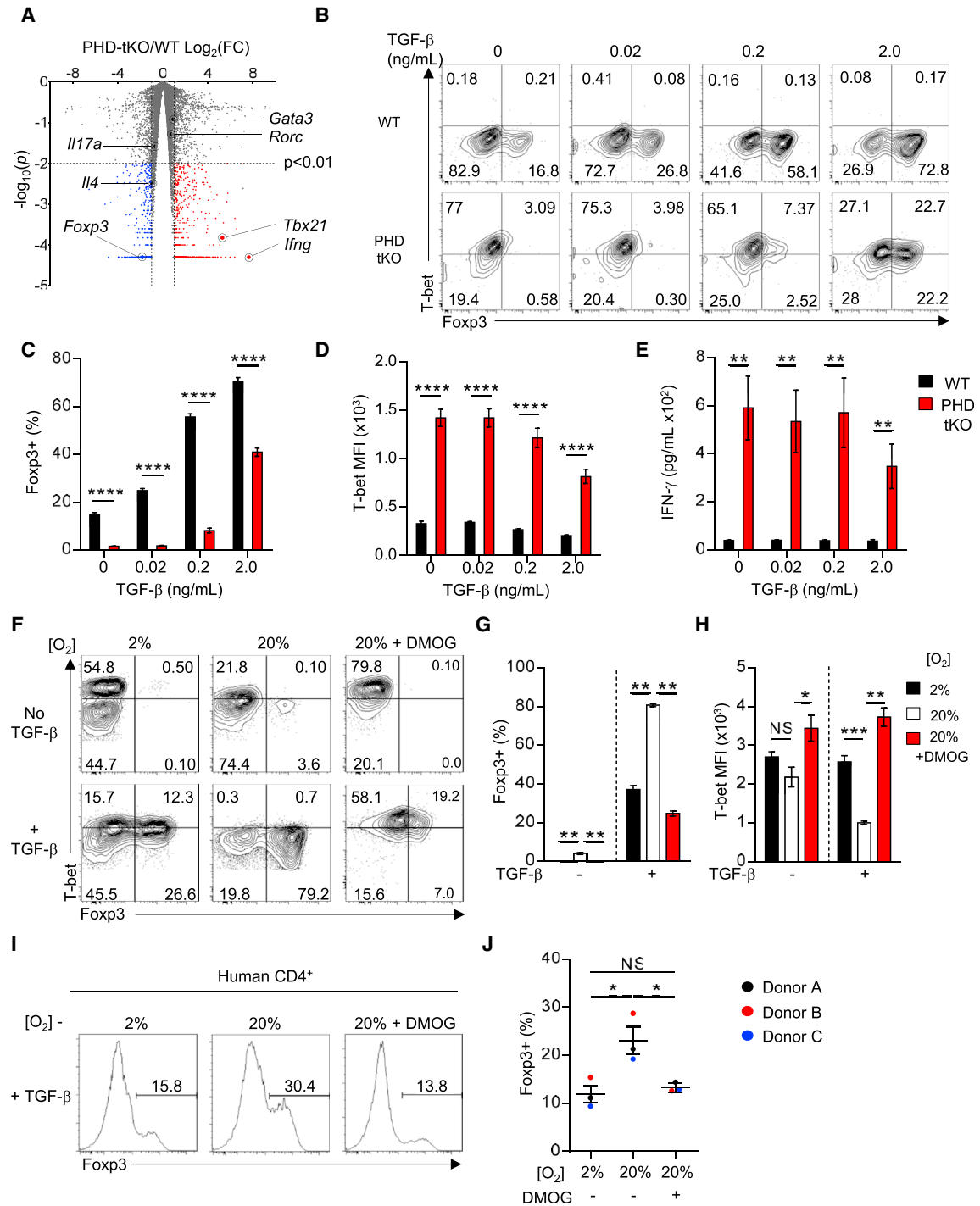
Figure 3. PHD Proteins Regulate Reciprocal iT$_{reg}$ and Th1 Differentiation Programs

(A) Volcano plot of expressed transcripts (RPKM ≥1) in PHD-tKO compared with WT CD4$^+$ T cells stimulated in vitro. Transcripts significantly (p < 0.01) overexpressed (FC ≥ 2, red) and under-expressed (FC ≤ 0.5, blue) in PHD-tKO cells are indicated.

(B–D) Foxp3 and T-bet expression in WT and PHD-tKO CD4$^+$ T cells stimulated in vitro in the presence of indicated amounts of TGF-β. Representative flow cytometry (B) and replicate values for Foxp3 (C) and T-bet (D) are shown.

(E) ELISA quantification of IFN-γ in culture supernatants from WT and PHD-tKO CD4$^+$ T cells stimulated as described in (B).

(F–H) Foxp3 and T-bet expression in WT CD4$^+$ T cells stimulated in vitro under the indicated environmental oxygen concentrations ± DMOG. Representative flow cytometry (F) and replicate values (G and H) shown.

(legend continued on next page)

iT$_{reg}$ cells (Figure S3D). Foxp3$^+$ T-bet$^+$ T$_{reg}$ cells exert suppressive function, especially in inflammatory contexts (Koch et al., 2009). Consistently, fluorescence-activated cell sorting (FACS)-purified Foxp3-GFP$^+$ iT$_{reg}$ cells generated in the presence of DMOG, which express high levels of T-bet, were as suppressive in vitro as T-bet^{Lo} iT$_{reg}$ cells (Figures S3E and S3F).

Downstream substrates of PHD enzymatic activity including HIF1α have been implicated in Th17 differentiation and CD8$^+$ T cell effector function (Dang et al., 2011; Doedens et al., 2013). We evaluated whether PHD proteins restrain differentiation and function of these lineages. IL-17A production was similar in CD4$^+$ T cells isolated from the lung and small intestine LP of WT and PHD-tKO mice (Figure S3G). Moreover, no differences in RORγt expression or IL-17A production were detected between WT and PHD-tKO T cells stimulated under Th17 polarizing conditions in vitro (Figure S3H). Consistent with the increased frequency of effector CD8$^+$ T cells in PHD-tKO mice, we observed increased terminal differentiation and production of cytolytic molecules among PHD-tKO CD8$^+$ T cells stimulated in vitro (Figures S3I and S3J).

Collectively, these results demonstrate that PHD proteins function within the CD4$^+$ T cell lineage to promote iT$_{reg}$ cell differentiation while restraining the differentiation of Th1 cells. Within the CD8$^+$ T cell lineage, PHD proteins restrain the acquisition of effector cytokine and cytolytic functions.

Extracellular Oxygen Promotes iT$_{reg}$ Cell Differentiation in a PHD-Dependent Manner

Local environmental factors influence immune responses in a site-specific manner. Orally ingested food antigens, vitamins, and commensal microbes and their metabolite byproducts promote local iT$_{reg}$ cell differentiation in the small intestine (Arpaia et al., 2013; Atarashi et al., 2011; Mucida et al., 2005; Sun et al., 2007). T cells in the lung reside in an oxygen rich environment (≥ 13% O$_2$) (Semenza, 2010). We asked whether extracellular oxygen availability influences the efficiency of iT$_{reg}$ and Th1 cell differentiation. WT CD4$^+$ T cells were stimulated in vitro under fixed extracellular oxygen concentrations. Cells stimulated under higher oxygen tensions demonstrated increased iT$_{reg}$ and reduced Th1 cell differentiation, and this phenomenon was dependent on the oxygen-sensing PHD proteins (Figure 3F–3H). High extracellular oxygen also promoted human iT$_{reg}$ cell differentiation in a PHD-dependent manner (Figures 3I and 3J). Thus, PHD proteins enable T-cell-intrinsic detection of environmental oxygen, which influences reciprocal iT$_{reg}$ and Th1 cell differentiation efficiency.

PHD Proteins Are Functionally Redundant in T Lymphocytes

Many biologic systems exhibit functional redundancy. We asked whether a single PHD protein is functionally predominant in T cells or if they function in a redundant manner. We generated mice with T-cell-specific deletions of one, two, or all three PHD proteins. We hypothesized that if any one PHD protein was functionally predominant, then removal of this factor should phenocopy the effect of deletion of all three. Deletion of one or two PHD proteins did not significantly affect IFN-γ production or Nrp-1^{Lo} T$_{reg}$ cell frequency among pulmonary CD4$^+$ T cells (Figures 4A and 4B). Only loss of all three PHD proteins resulted in a dramatic increase in the pulmonary IFN-γ$^+$ T$_{eff}$ to Nrp-1^{Lo} T$_{reg}$ cell ratio (Figure 4E). Elevated IFN-γ production in pulmonary CD8$^+$ T cells was detected only when all three PHD proteins were ablated (Figures 4C and 4D). Deletion of one PHD protein or the combined removal of PHD1/PHD2 or PHD1/PHD3 did not affect iT$_{reg}$ cell differentiation in vitro. PHD2/3 dKO T cells demonstrated a modest reduction in iT$_{reg}$ cell differentiation and reciprocal increase in Th1 cell differentiation. However, this defect was most pronounced in PHD-tKO cells (Figures S4A–S4C). Collectively, these results provide evidence that PHD proteins function redundantly in T cells.

PHD Proteins Repress HIF-Driven Glycolytic Metabolism to Mediate T Cell Fate Specification

We next asked how PHD proteins mediate reciprocal iT$_{reg}$ and Th1 cellular differentiation programs. Gene set enrichment analysis (GSEA) of the global transcriptional differences between PHD-tKO and WT CD4$^+$ T cells activated in vitro revealed significant enrichment of genes involved in hypoxic responses and transcriptional targets of hypoxia-inducible factors in PHD-tKO cells (Figure S5A). Nuclear accumulation of HIFα proteins correlates inversely with PHD hydroxylase activity (Kaelin and Ratcliffe, 2008). We therefore measured the dynamics of HIF1α mRNA and protein expression in WT and PHD-tKO T cells. Naive and activated WT and PHD-tKO CD4$^+$ T cells had similar expression of *Hif1a* mRNA (Figure S5B). HIF1α protein expression was similar in naive cells but significantly elevated in PHD-tKO T cells upon activation (Figure S5C). Consistent with their functional redundancy, each PHD protein limited HIF1α accumulation in T cells (Figure 5A). Furthermore, HIF1α accumulation was suppressed in CD4$^+$ T cells stimulated in high oxygen environments in a PHD-dependent manner (Figure 5B).

We asked whether PHD-mediated suppression of HIF1α accumulation is required for appropriate control of iT$_{reg}$ and Th1 cell differentiation. We analyzed HIF1α, Foxp3, and T-bet protein expression in CD4$^+$ T cells isolated from each PHD KO genotype. HIF1α accumulation inversely correlated with iT$_{reg}$ cell differentiation (Figure 5C) and positively correlated with Th1 effector cell differentiation (Figure 5D). Moreover, loss of HIF1α and HIF2α partially rescued iT$_{reg}$ cell differentiation and reversed excessive Th1 differentiation when the enzymatic activity of PHD proteins was inhibited using DMOG (Figures 5E–5G). Loss of HIF1α alone only partially reversed the phenotype induced by DMOG, while loss of HIF2α had little effect on the phenotype (Figures 5F, 5G, S5D, and S5E). Thus, PHD proteins

---

(I–J) Foxp3$^+$ iT$_{reg}$ fate specification of human CD4$^+$ T cells stimulated in vitro under the indicated environmental oxygen concentrations ± DMOG. Representative flow cytometry histograms (I) and replicate values are shown (J).

Data are representative of two or more independent experiments. Bars and error represent mean ± SEM of replicate measurements. *p < 0.05, **p < 0.01, ***p < 0.001, ****p < 0.0001 (Student's t test).

See also Figure S3.
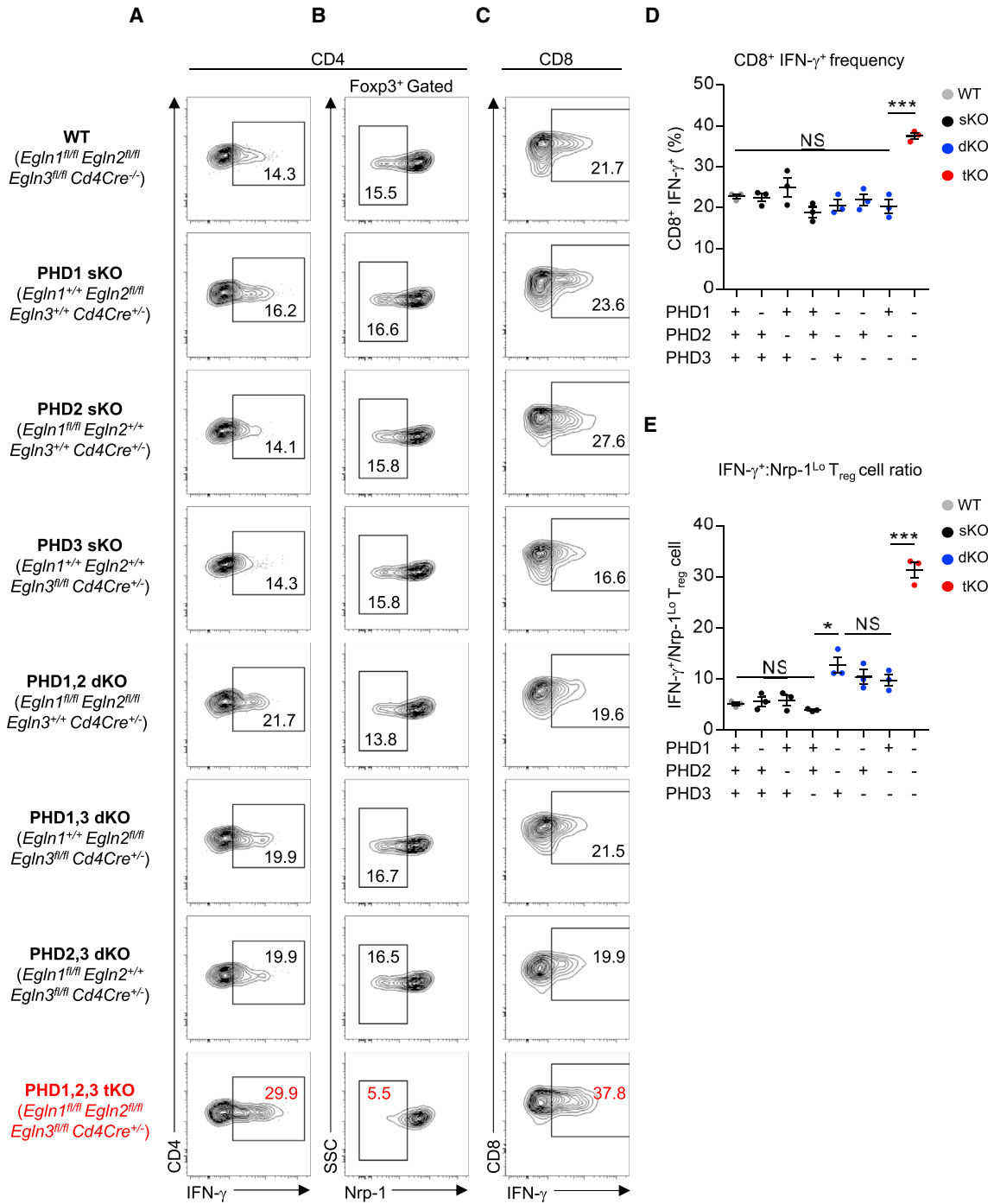
**Figure 4. PHD Proteins Are Functionally Redundant in T Lymphocytes**

(A and B) Phenotype of pulmonary CD4^{+} T cells in mice with indicated PHD protein deficiency. Representative flow cytometry of IFN-γ expression (A) and Nrp-1 expression by Foxp3^{+} T_reg cells (B).

(C and D) IFN-γ expression by pulmonary CD8^{+} T cells in mice with indicated PHD protein deficiency. Representative flow cytometry (C) and replicate values (D) are shown.

(E) Ratio of CD4^{+} IFN-γ^{+} T_eff cells to Nrp-1[Lo] Foxp3^{+} T_reg cells of total pulmonary CD4^{+} T cells in mice with the indicated PHD protein deficiency.

Data are representative of two or more independent experiments with three or more mice per genotype. Bars and error represent mean ± SEM of replicate measurements. *p < 0.05, ***p < 0.001 (Student's t test).

See also Figure S4.
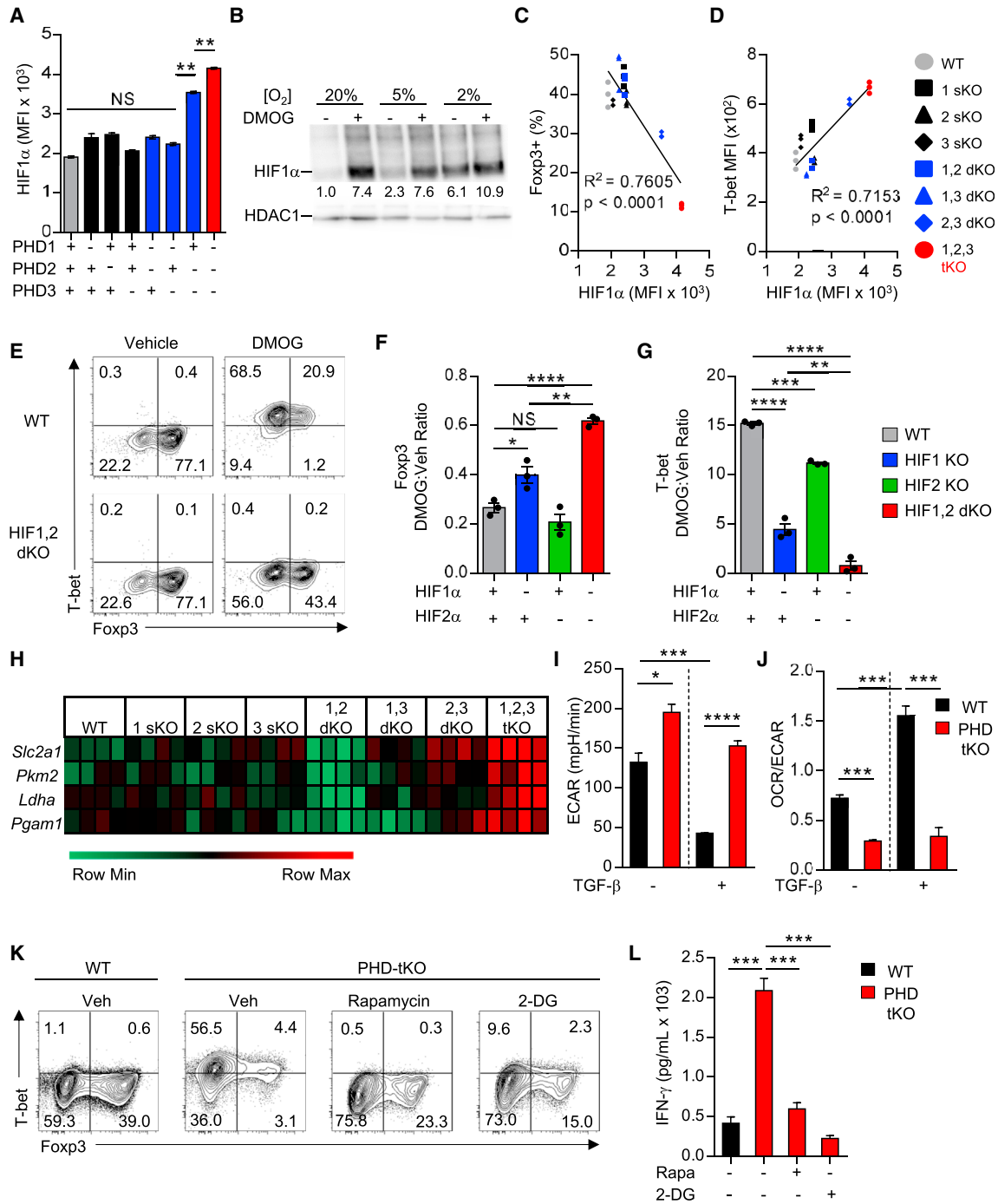
Figure 5. PHD Proteins Control T Cell Differentiation through Repression of HIF-Driven Glycolytic Metabolism

(A) Flow cytometry detection of HIF1α expression in CD4⁺ T cells isolated from mice with the indicated PHD KO genotype and stimulated in vitro. Average HIF1α MFI is shown.

(B) Immunoblot of HIF1α and HDAC1 from nuclear lysate of WT CD4⁺ T cells stimulated in vitro in the indicated environmental oxygen concentrations ± DMOG. Numbers indicate densitometry quantification of HIF1α band intensity relative to HDAC1 loading control. All values are normalized to HIF1α/HDAC1 density in cells stimulated in 20% oxygen in the absence of DMOG (lane 1).

(C and D) Correlation between HIF1α and Foxp3 (C) and T-bet (D) expression in CD4⁺ T cells isolated from the indicated PHD KO genotype and stimulated as described in (A).

(E) Representative flow cytometry of Foxp3 and T-bet expression in WT and HIF1,2α double-knockout (HIF1,2 dKO) CD4⁺ T cells stimulated in vitro in the presence of TGF-β ± DMOG.

(legend continued on next page)

regulate CD4$^+$ T cell differentiation in part by controlling the expression of HIFα proteins.

HIF transcriptional activity drives expression of genes involved in multiple cellular programs including glycolysis. Expression of components of the glycolytic machinery was elevated in PHD-tKO and DMOG-treated WT T cells in a HIFα-dependent manner (Figures 5H, S5F, and S5G). T cells stimulated in the presence of TGF-β demonstrated a PHD-dependent reduction in extracellular acidification rate (ECAR), a measure of glycolytic activity (Figure 5I). PHD-tKO CD4$^+$ T cells demonstrated increased glucose uptake (Figure S5H) and adopted an anaerobic metabolic signature (Figure 5J). PHD proteins also restrained glycolysis in CD8$^+$ T cells (Figure S5I).

Metabolic programs direct T cell fate specification and effector function (Chang et al., 2013; Cui et al., 2015; Gerriets et al., 2015). We asked whether PHD-mediated repression of glycolysis is required for appropriate iT$_{reg}$ and Th1 cell specification. Strikingly, pharmacological blockade of mTOR-driven glycolytic programs or glycolysis with rapamycin and 2-deoxy-glucose, respectively, completely abrogated spontaneous Th1 differentiation and IFN-γ production and partially restored iT$_{reg}$ cell differentiation in PHD-tKO T cells (Figures 5K, 5L, and S5J). Collectively, these findings suggest that PHD proteins coordinate a transcriptional and metabolic program that regulates the reciprocal differentiation of Th1 and iT$_{reg}$ cells.

T-Cell-Intrinsic Expression of PHD Proteins Licenses Tumor Colonization of the Lung

We found that PHD proteins coordinate a T-cell-intrinsic immunoregulatory program to sustain tolerance against harmless environmental antigens in the lung. We reasoned that infiltrating pre-metastatic cancer cells might resemble innocuous foreign antigens through their expression of mutated neoantigenic epitopes. We therefore hypothesized that PHD proteins limit effector responses against infiltrating tumor cells in the lung. We evaluated the ability of circulating tumor cells to colonize lungs of WT and PHD-tKO mice. As a control, we also evaluated subcutaneous tumor growth. WT and PHD-tKO mice were injected with B16 melanoma tumors subcutaneously in the flank and intravenously (i.v.) through the tail vein to introduce tumor cells at each site within the same animal (Figure 6A). Strikingly, while subcutaneous tumor growth was similar in WT and PHD-tKO mice (Figure 6B), PHD-tKO mice were significantly protected from tumor colonization in the lung. PHD-tKO animals had fewer detectable lung tumors upon gross and microscopic evaluation (Figures 6C and 6D), resulting in a significant reduction in total pulmonary tumor burden (Figure 6E).

We next analyzed the immune phenotype of CD4$^+$ T cells in WT and PHD-tKO mice that were injected i.v. with B16 melanoma. The frequency of splenic T$_{reg}$ cells was similar in WT and PHD-tKO mice (Figure 6F). However, we observed an increase in the frequency of pulmonary T$_{reg}$ cells following i.v. tumor administration that was absent in PHD-tKO mice (Figures 6F and 6G). Additionally, we detected increased frequencies of IFN-γ-expressing pulmonary CD4$^+$ T cells in PHD-tKO mice compared to WT controls upon tumor colonization (Figures 6F and 6H).

Th1 cells play an important role in orchestrating anti-tumor immunity (Pardoll and Topalian, 1998). We asked whether PHD proteins support pulmonary tumor colonization through suppression of IFN-γ-mediated anti-tumor immunity. PHD-tKO mice were injected intravenously with B16 melanoma and received IFN-γ neutralizing or control antibodies at serial time points following tumor implantation. Strikingly, the protection from lung tumor colonization observed in PHD-tKO mice was abrogated by IFN-γ neutralization (Figure 6I). Thus, PHD proteins limit IFN-γ-mediated tumor clearance in the lung.

These results indicate that T-cell-intrinsic expression of PHD proteins restrains anti-tumor immunity in the lung, thus creating favorable conditions for metastatic tumor colonization.

Inhibition of PHD Proteins Improves Adoptive Cell Transfer Immunotherapy

Our findings suggested that inhibition of PHD proteins in T cells may improve the efficacy of cancer immunotherapy. To explore this hypothesis, we utilized the TRP-1 TCR-transgenic system to model adoptive cell transfer immunotherapy (ACT) (Muranski et al., 2008). In this model, antigen-specific TRP-1 CD4$^+$ T cells are expanded ex vivo and transferred into mice bearing established subcutaneous or pulmonary B16 melanoma tumors (Figure 7A).

We expanded TRP-1 CD4$^+$ T cells in the presence or absence of DMOG. DMOG-treated cultures (TRP-1 DMOG) demonstrated increased Th1 differentiation and IFN-γ production compared to vehicle-treated cultures (TRP-1 VEH) (Figures 7A and 7B). Cells were adoptively transferred into WT mice that had established B16 melanoma metastases in the lung. Consistent with their enhanced effector phenotype at the time of infusion, TRP-1 DMOG cells mediated superior clearance of lung metastases (Figures 7C and 7D). Additionally, TRP-1 DMOG cells mediated superior regression of established subcutaneous tumors (Figure 7E). This led to an increase in overall survival of tumor-bearing mice (Figure 7F). We have previously found that Th1 cells are more effective than Th0 cells at inducing tumor

(F and G) Foxp3 (F) and T-bet (G) expression in CD4$^+$ T cells isolated from HIF1α sKO, HIF2α sKO, HIF1,2α dKO, or WT mice and stimulated in vitro in the presence of TGF-β ± DMOG. Protein expression levels in DMOG-treated cells are normalized to vehicle. Black dots represent biologic replicates.

(H) mRNA expression of glycolytic genes in CD4$^+$ T cells isolated from the indicated PHD KO genotype and stimulated in vitro. Heatmap normalized to row minimum and maximum for each gene.

(I and J) ECAR (I) and OCR:ECAR ratio (J) as determined by Seahorse bioassay in CD4$^+$ T cells isolated from WT and PHD-tKO mice and stimulated in vitro.

(K) Foxp3 and T-bet expression in WT and PHD-tKO CD4$^+$ T cells stimulated in vitro in the presence of TGF-β with or without the addition of compounds which inhibit glycolysis directly (2-DG) or indirectly (Rapamycin).

(L) IFN-γ ELISA from supernatants of WT and PHD-tKO CD4$^+$ T cells stimulated in vitro as described in (K).

Data are representative of two or more independent experiments. Bars and error represent mean ± SEM of replicate measurements. *p < 0.05, **p < 0.01, ***p < 0.001, ****p < 0.0001 (Student's t test).

See also Figure S5.
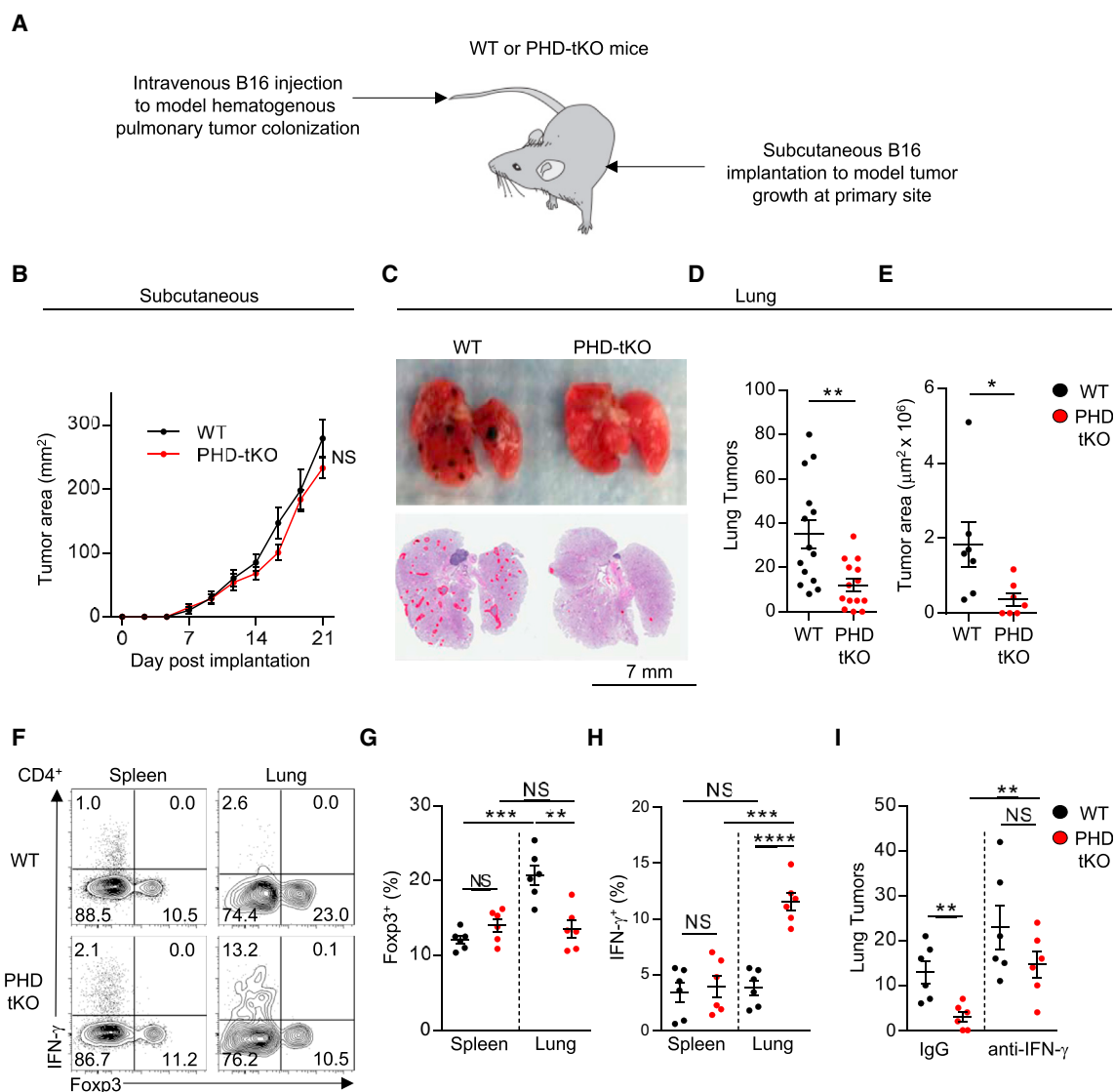
Figure 6. T-Cell-Intrinsic Expression of PHD Proteins Licenses Tumor Colonization of the Lung

(A) Experimental schema of primary subcutaneous and secondary pulmonary tumor colonization in WT and PHD-tKO mice.

(B) Growth kinetics of subcutaneous B16 melanoma in PHD-tKO or WT mice.

(C) Gross morphology and H&E analysis of lungs from PHD-tKO or WT mice following intravenous injection of B16 melanoma. Micrometastatic lesions are outlined in red.

(D and E) Quantification of total metastatic nodules (D) and total area of tumor burden (E) in lung H&E sections from mice described in (C).

(F–H) Foxp3 and IFN-γ expression in CD4$^+$ T lymphocytes isolated from the spleen and lungs of PHD-tKO and WT mice following i.v. B16 melanoma injection. Representative flow cytometry (F) and replicate values for Foxp3 (G) and IFN-γ (H) are shown.

(I) Quantification of pulmonary tumor nodules in PHD-tKO or WT mice injected intravenously with B16 melanoma and administered IFN-γ neutralizing or immunoglobulin G (IgG) control antibodies.

Data are representative of two or more independent experiments with more than five mice per group. Bars and error represent mean ± SEM of replicate measurements. *p < 0.05, **p < 0.01, ***p < 0.001, ****p < 0.0001 (Student's t test).

rejection (Muranski et al., 2008). Augmented anti-tumor function in mice administered TRP-1 DMOG cells is consistent with the induction of a Th1 phenotype in these cells. Indeed, TRP-1 DMOG cells were as effective in mediating tumor regression as cells polarized under conventional Th1 cell specifying conditions (Figures S6A and S6B). Thus, inhibition of PHD proteins provides a novel strategy to enforce Th1 cell differentiation under conditions conventionally used for ACT, thereby providing a potential means to improve the efficacy of ACT.

DISCUSSION

In this study, we have demonstrated that three proteins comprising the PHD protein family function redundantly within
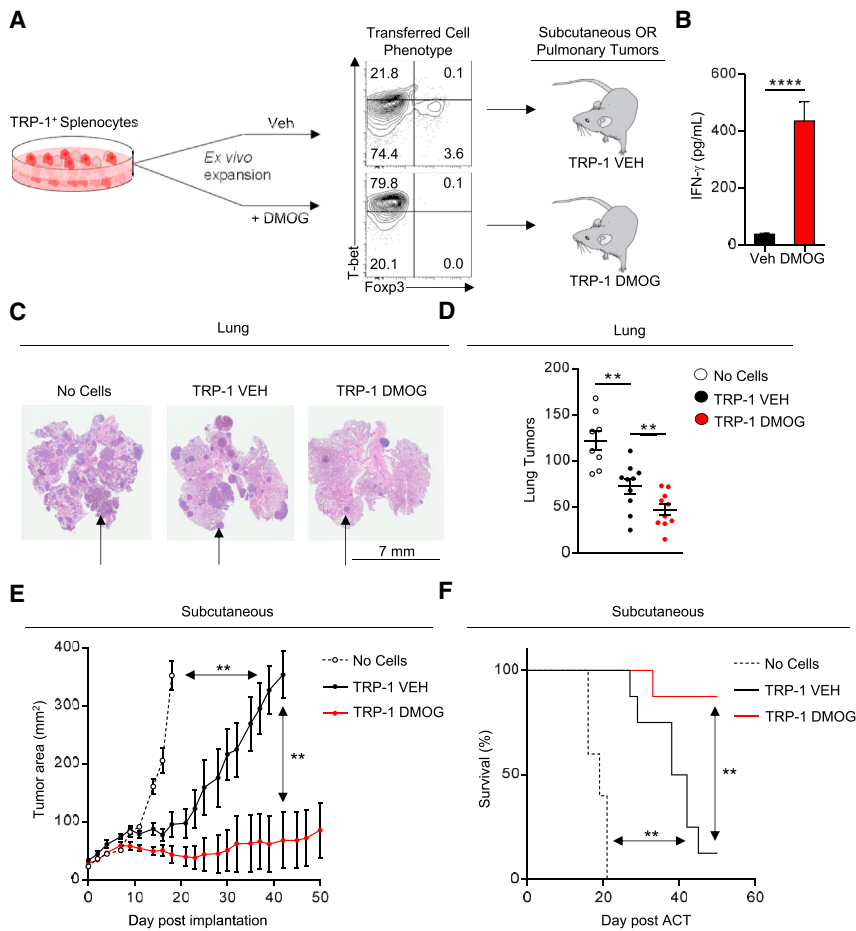
Figure 7. Inhibition of PHD Proteins Improves Adoptive Cell Transfer Immunotherapy

(A) Experimental schema of adoptive cell transfer immunotherapy (ACT). Pre-transfer levels of T-bet and Foxp3 expression is shown.

(B) IFN-γ ELISA from culture supernatants of TRP-1 splenocytes stimulated in vitro ± DMOG.

(C and D) Pulmonary tumor burden in mice receiving ACT of indicated cells. Representative H&E (C) and total lung tumor metastatic nodules (D) are shown. Black arrows indicate representative area of tumor burden.

(E and F) Subcutaneous tumor growth in mice receiving ACT of indicated cells. Tumor area (E) and overall survival (F) are shown. Survival significance was assessed by a log-rank Mantel-Cox test.

Data are representative of two or more independent experiments with more than five mice per group. Bars and error represent mean ± SEM of replicate measurements. **$p < 0.01$, ****$p < 0.0001$ (Student's t test).

See also Figure S6.

T cells to promote pulmonary immune homeostasis in the face of innocuous foreign antigens. However, this immuno-regulatory mechanism drives deleterious immunosuppression upon invasion of the lung by circulating tumor cells. Over a century ago, Stephen Paget developed the "seed and soil" hypothesis, according to which properties of pre-metastatic cancer cells ("seed") and secondary sites ("soil") are required for the development and distribution of cancer metastases. While many studies have focused on cancer cell-intrinsic programs that contribute to metastatic potential, our investigations indicate that PHD proteins function within T cells to establish the lung as an immunologically permissive metastatic site. These results provide an immunological basis for the predisposition of many cancers to metastasize to the lung.

It is reasonable to hypothesize that cancers preferentially metastasize to sites where local immune responses are suppressed. From an evolutionary perspective, the selective pressure to restrain pathologic inflammation likely outweighed the pressure to protect against tumor cell metastasis. T cells in the lung experience continuous exposure to innocuous foreign antigens. The default immune response against these stimuli is non-inflammatory and immunosuppressive. Our find-

ings reveal a T-cell-intrinsic program whereby the PHD proteins contribute to pulmonary tolerance by restraining inflammatory CD4$^+$ and CD8$^+$ T cell responses and permitting immunosuppressive iT$_{reg}$ cell differentiation. Infectious respiratory pathogens can bypass the "default state" as pathogen-associated molecular pattern antigens stimulate pulmonary dendritic cells to promote inflammatory T cell responses (Wikstrom and Stumbles, 2007). Elucidating whether PHD proteins influence T cell responses against respiratory pathogens will be an important area of investigation.

We observed a local PHD-dependent increase in T$_{reg}$ cell frequency and number following pulmonary challenge with HDM or B16 melanoma. Whether this is the result of de novo induction of antigen-specific iT$_{reg}$ cells, expansion of existing pulmonary T$_{reg}$ cells, or recruitment of T$_{reg}$ cells from distant sites is incompletely resolved. The antigen-driven increase in pulmonary T$_{reg}$ cells was absent in PHD-tKO animals, which have normal baseline tT$_{reg}$ cells but reduced iT$_{reg}$ cells and differentiation potential. These findings raise the possibility that de novo specification of iT$_{reg}$ cells following exposure to innocuous antigens or colonizing cancer cells is required to maintain pulmonary tolerance and support metastasis to the lung.

PHD proteins restrain CD4$^+$ and CD8$^+$ T cell effector function in many tissues, yet this was most pronounced in the lung—even when compared to mediastinal lymph nodes. However, these data do not exclude the possibility that PHD proteins also play a role in effector cell specification in secondary lymphoid organs. Moreover, we only detected increased numbers of CD4$^+$ and CD8$^+$ T cells in the lungs of PHD-tKO mice, but not other organs, suggesting that PHD proteins are

involved in lymphocyte trafficking or site-specific survival and proliferation. This may be related to increased T-bet expression, which drives T cell effector differentiation and localization to peripheral non-lymphoid tissues (Joshi et al., 2007; Lord et al., 2005). The development of lung pathology in PHD-tKO mice is likely caused by inappropriate inflammatory responses against innocuous antigens in a well-oxygenated tissue. T cells in the gut also experience continuous antigen exposure. However, in the less well oxygenated gut microenvironment, PHD-independent mechanisms are the predominant mediators of tolerance. PHD proteins also appear dispensable for steady-state immune tolerance in sterile tissues. However, PHD proteins might restrain inflammation in these organs upon the introduction of antigen, such as an infectious pathogen or a metastasizing cancer cell.

PHD proteins limit HIF-driven glycolytic programs to inhibit spontaneous Th1 differentiation in conditions that promote iT$_{reg}$ cell commitment. PHD proteins also suppress necrosis factor κB (NF-κB) signaling through the hydroxylation and inactivation of IKKβ (Cummins et al., 2006). Thus, in addition to constitutive HIF activity, PHD-tKO or DMOG-treated WT cells may experience increased NF-κB signaling, which in excess can prevent iT$_{reg}$ cell differentiation (Molinero et al., 2011). Elucidating new and existing PHD substrates and dissecting the contributions of each in T cell differentiation will be an important area of future study.

Genetic and pharmacological inhibition of T-cell-intrinsic PHD proteins limits tumor dissemination into the lung and improves the efficacy of ACT. Inhibition of PHD proteins could offer a viable clinical strategy to limit lung metastasis. However, systemic administration of a PHD inhibitor may not be effective. HIF has been shown to increase proliferation in some cancer types (Keith et al., 2012). HIF also promotes the development of immunosuppressive macrophages (Colegio et al., 2014; Doedens et al., 2010). Instead, a clinical strategy that permits PHD inhibition selectively in T cells, such as ACT, should be considered. In models of ACT that depend on therapeutic vaccination, inhibition of glycolysis in vitro improves expansion and anti-tumor efficacy in vivo (Sukumar et al., 2013). However, in the non-vaccine setting, which is more similar to ACT protocols in humans, enforcing effector capacity ex vivo might improve the anti-tumor efficacy of tumor-specificlymphocytes. Promoting glycolytic metabolism might also improve their ability to compete for nutrients in the tumor microenvironment (Chang et al., 2015; Ho et al., 2015). Consistently, T cells expanded in the presence of DMOG were highly glycolytic, spontaneously acquired Th1 effector properties, and ultimately mediated superior tumor regression in mouse models of ACT. Addition of a PHD inhibitor to established clinical expansion protocols for human ACT using tumor-infiltrating lymphocytes (TILs) or chimeric antigen receptor (CAR)-transduced T cells is a feasible and potentially effective therapeutic strategy to improve the functional quality of tumor-specific T cells.

In summary, our findings provide an understanding of how site-specific immunoregulatory mechanisms contribute to the permissivity of distinct anatomical locations to tumor colonization in a manner amenable to therapeutic intervention.

STAR★METHODS

Detailed methods are provided in the online version of this paper and include the following:

- KEY RESOURCES TABLE
- CONTACT FOR REAGENT AND RESOURCE SHARING
- EXPERIMENTAL MODEL AND SUBJECT DETAILS
  - Mice
- METHOD DETAILS
  - In Vitro T Cell Differentiation
  - Histopathology
  - House Dust Mite Airway Challenge
  - Antibodies and Flow Cytometry
  - RNA Sequencing and Analysis
  - Autoantibody Enzyme-Linked Immunosorbent Assay
  - Quantitative Reverse-Transcription Polymerase Chain Reaction
  - Immunoblot Analysis
  - Bone Marrow Chimeras
  - In Vivo iT$_{reg}$ Induction
  - In Vivo T$_{reg}$ Stability
  - In Vitro T$_{reg}$ Stability
  - In Vitro Suppression Assay
  - Extracellular Acidification Rate and Glucose Uptake
  - Foxp3 TSDR Methylation
  - Experimental Metastasis
  - Adoptive Cell Transfer
- QUANTIFICATION AND STATISTICAL ANALYSIS
- DATA AND SOFTWARE AVAILABILITY
  - Data Resources

SUPPORTING CITATIONS

The following reference appears in the Supplemental Information: Kim and Salzberg, 2011.

REFERENCES

Arpaia, N., Campbell, C., Fan, X., Dikiy, S., van der Veeken, J., deRoos, P., Liu, H., Cross, J.R., Pfeffer, K., Coffer, P.J., and Rudensky, A.Y. (2013). Metabolites produced by commensal bacteria promote peripheral regulatory T-cell generation. Nature *504*, 451–455.

Atarashi, K., Tanoue, T., Shima, T., Imaoka, A., Kuwahara, T., Momose, Y., Cheng, G., Yamasaki, S., Saito, T., Ohba, Y., et al. (2011). Induction of colonic regulatory T cells by indigenous Clostridium species. Science *331*, 337–341.

Bluestone, J.A., and Abbas, A.K. (2003). Natural versus adaptive regulatory T cells. Nat. Rev. Immunol. *3*, 253–257.

Bruick, R.K., and McKnight, S.L. (2001). A conserved family of prolyl-4-hydroxylases that modify HIF. Science *294*, 1337–1340.

Chang, C.H., Curtis, J.D., Maggi, L.B., Jr., Faubert, B., Villarino, A.V., O'Sullivan, D., Huang, S.C., van der Windt, G.J., Blagih, J., Qiu, J., et al. (2013). Post-transcriptional control of T cell effector function by aerobic glycolysis. Cell *153*, 1239–1251.

Chang, C.H., Qiu, J., O'Sullivan, D., Buck, M.D., Noguchi, T., Curtis, J.D., Chen, Q., Gindin, M., Gubin, M.M., van der Windt, G.J., et al. (2015). Metabolic competition in the tumor microenvironment is a driver of cancer progression. Cell *162*, 1229–1241.

Chen, W., Jin, W., Hardegen, N., Lei, K.J., Li, L., Marinos, N., McGrady, G., and Wahl, S.M. (2003). Conversion of peripheral CD4+CD25– naive T cells to CD4+CD25+ regulatory T cells by TGF-beta induction of transcription factor Foxp3. J. Exp. Med. *198*, 1875–1886.

Colegio, O.R., Chu, N.Q., Szabo, A.L., Chu, T., Rhebergen, A.M., Jairam, V., Cyrus, N., Brokowski, C.E., Eisenbarth, S.C., Phillips, G.M., et al. (2014). Functional polarization of tumour-associated macrophages by tumour-derived lactic acid. Nature *513*, 559–563.

Cui, G., Staron, M.M., Gray, S.M., Ho, P.C., Amezquita, R.A., Wu, J., and Kaech, S.M. (2015). IL-7-induced glycerol transport and TAG synthesis promotes memory CD8+ T cell longevity. Cell *161*, 750–761.

Cummins, E.P., Berra, E., Comerford, K.M., Ginouves, A., Fitzgerald, K.T., Seeballuck, F., Godson, C., Nielsen, J.E., Moynagh, P., Pouyssegur, J., and Taylor, C.T. (2006). Prolyl hydroxylase-1 negatively regulates IkappaB kinase-beta, giving insight into hypoxia-induced NFkappaB activity. Proc. Natl. Acad. Sci. USA *103*, 18154–18159.

Dang, E.V., Barbi, J., Yang, H.Y., Jinasena, D., Yu, H., Zheng, Y., Bordman, Z., Fu, J., Kim, Y., Yen, H.R., et al. (2011). Control of T(H)17/T(reg) balance by hypoxia-inducible factor 1. Cell *146*, 772–784.

de Heer, H.J., Hammad, H., Soullié, T., Hijdra, D., Vos, N., Willart, M.A., Hoogsteden, H.C., and Lambrecht, B.N. (2004). Essential role of lung plasmacytoid dendritic cells in preventing asthmatic reactions to harmless inhaled antigen. J. Exp. Med. *200*, 89–98.

Doedens, A.L., Stockmann, C., Rubinstein, M.P., Liao, D., Zhang, N., DeNardo, D.G., Coussens, L.M., Karin, M., Goldrath, A.W., and Johnson, R.S. (2010). Macrophage expression of hypoxia-inducible factor-1 alpha suppresses T-cell function and promotes tumor progression. Cancer Res. *70*, 7465–7475.

Doedens, A.L., Phan, A.T., Stradner, M.H., Fujimoto, J.K., Nguyen, J.V., Yang, E., Johnson, R.S., and Goldrath, A.W. (2013). Hypoxia-inducible factors enhance the effector responses of CD8(+) T cells to persistent antigen. Nat. Immunol. *14*, 1173–1182.

Epstein, A.C., Gleadle, J.M., McNeill, L.A., Hewitson, K.S., O'Rourke, J., Mole, D.R., Mukherji, M., Metzen, E., Wilson, M.I., Dhanda, A., et al. (2001). C. elegans EGL-9 and mammalian homologs define a family of dioxygenases that regulate HIF by prolyl hydroxylation. Cell *107*, 43–54.

Floess, S., Freyer, J., Siewert, C., Baron, U., Olek, S., Polansky, J., Schlawe, K., Chang, H.D., Bopp, T., Schmitt, E., et al. (2007). Epigenetic control of the foxp3 locus in regulatory T cells. PLoS Biol. *5*, e38.

Gavin, M.A., Rasmussen, J.P., Fontenot, J.D., Vasta, V., Manganiello, V.C., Beavo, J.A., and Rudensky, A.Y. (2007). Foxp3-dependent programme of regulatory T-cell differentiation. Nature *445*, 771–775.

Gerriets, V.A., Kishton, R.J., Nichols, A.G., Macintyre, A.N., Inoue, M., Ilkayeva, O., Winter, P.S., Liu, X., Priyadharshini, B., Slawinska, M.E., et al. (2015). Metabolic programming and PDHK1 control CD4+ T cell subsets and inflammation. J. Clin. Invest. *125*, 194–207.

Gruber, M., Hu, C.J., Johnson, R.S., Brown, E.J., Keith, B., and Simon, M.C. (2007). Acute postnatal ablation of Hif-2alpha results in anemia. Proc. Natl. Acad. Sci. USA *104*, 2301–2306.

Ho, P.C., Bihuniak, J.D., Macintyre, A.N., Staron, M., Liu, X., Amezquita, R., Tsui, Y.C., Cui, G., Micevic, G., Perales, J.C., et al. (2015). Phosphoenolpyruvate is a metabolic checkpoint of anti-tumor T cell responses. Cell *162*, 1217–1228.

Holt, P.G., Strickland, D.H., Wikström, M.E., and Jahnsen, F.L. (2008). Regulation of immunological homeostasis in the respiratory tract. Nat. Rev. Immunol. *8*, 142–152.

Jaakkola, P., Mole, D.R., Tian, Y.M., Wilson, M.I., Gielbert, J., Gaskell, S.J., von Kriegsheim, A., Hebestreit, H.F., Mukherji, M., Schofield, C.J., et al. (2001). Targeting of HIF-alpha to the von Hippel-Lindau ubiquitylation complex by O2-regulated prolyl hydroxylation. Science *292*, 468–472.

Josefowicz, S.Z., Niec, R.E., Kim, H.Y., Treuting, P., Chinen, T., Zheng, Y., Umetsu, D.T., and Rudensky, A.Y. (2012). Extrathymically generated regulatory T cells control mucosal TH2 inflammation. Nature *482*, 395–399.

Joshi, N.S., Cui, W., Chandele, A., Lee, H.K., Urso, D.R., Hagman, J., Gapin, L., and Kaech, S.M. (2007). Inflammation directs memory precursor and short-lived effector CD8(+) T cell fates via the graded expression of T-bet transcription factor. Immunity *27*, 281–295.

Kaelin, W.G., Jr., and Ratcliffe, P.J. (2008). Oxygen sensing by metazoans: the central role of the HIF hydroxylase pathway. Mol. Cell *30*, 393–402.

Keith, B., Johnson, R.S., and Simon, M.C. (2012). HIF1α and HIF2α: sibling rivalry in hypoxic tumour growth and progression. Nat. Rev. Cancer *12*, 9–22.

Kim, D., and Salzberg, S.L. (2011). TopHat-Fusion: An algorithm for discovery of novel fusion transcripts. Genome Biol. *12*, R72.

Koch, M.A., Tucker-Heard, G., Perdue, N.R., Killebrew, J.R., Urdahl, K.B., and Campbell, D.J. (2009). The transcription factor T-bet controls regulatory T cell homeostasis and function during type 1 inflammation. Nat. Immunol. *10*, 595–602.

Koch, M.A., Thomas, K.R., Perdue, N.R., Smigiel, K.S., Srivastava, S., and Campbell, D.J. (2012). T-bet(+) Treg cells undergo abortive Th1 cell differentiation due to impaired expression of IL-12 receptor β2. Immunity *37*, 501–510.

Lee, J.H., Elly, C., Park, Y., and Liu, Y.C. (2015). E3 ubiquitin ligase VHL regulates hypoxia-inducible factor-1α to maintain regulatory T cell stability and suppressive capacity. Immunity *42*, 1062–1074.

Li, M.O., Sanjabi, S., and Flavell, R.A. (2006). Transforming growth factor-beta controls development, homeostasis, and tolerance of T cells by regulatory T cell-dependent and -independent mechanisms. Immunity *25*, 455–471.

Lord, G.M., Rao, R.M., Choe, H., Sullivan, B.M., Lichtman, A.H., Luscinskas, F.W., and Glimcher, L.H. (2005). T-bet is required for optimal proinflammatory CD4+ T-cell trafficking. Blood *106*, 3432–3439.

Massagué, J., and Obenauf, A.C. (2016). Metastatic colonization by circulating tumour cells. Nature *529*, 298–306.

Minn, A.J., Gupta, G.P., Siegel, P.M., Bos, P.D., Shu, W., Giri, D.D., Viale, A., Olshen, A.B., Gerald, W.L., and Massagué, J. (2005). Genes that mediate breast cancer metastasis to lung. Nature *436*, 518–524.

Molinero, L.L., Miller, M.L., Evaristo, C., and Alegre, M.L. (2011). High TCR stimuli prevent induced regulatory T cell differentiation in a NF-κB-dependent manner. J. Immunol. *186*, 4609–4617.

Mucida, D., Kutchukhidze, N., Erazo, A., Russo, M., Lafaille, J.J., and Curotto de Lafaille, M.A. (2005). Oral tolerance in the absence of naturally occurring Tregs. J. Clin. Invest. *115*, 1923–1933.

Muranski, P., Boni, A., Antony, P.A., Cassard, L., Irvine, K.R., Kaiser, A., Paulos, C.M., Palmer, D.C., Touloukian, C.E., Ptak, K., et al. (2008). Tumor-specific Th17-polarized cells eradicate large established melanoma. Blood *112*, 362–373.

Pardoll, D.M., and Topalian, S.L. (1998). The role of CD4+ T cell responses in antitumor immunity. Curr. Opin. Immunol. *10*, 588–594.

Ryan, H.E., Poloni, M., McNulty, W., Elson, D., Gassmann, M., Arbeit, J.M., and Johnson, R.S. (2000). Hypoxia-inducible factor-1alpha is a positive factor in solid tumor growth. Cancer Res. *60*, 4010–4015.

Sakaguchi, S., Fukuma, K., Kuribayashi, K., and Masuda, T. (1985). Organ-specific autoimmune diseases induced in mice by elimination of T cell subset. I. Evidence for the active participation of T cells in natural self-tolerance; deficit of a T cell subset as a possible cause of autoimmune disease. J. Exp. Med. *161*, 72–87.

Semenza, G.L. (2010). Oxygen homeostasis. Wiley Interdisc. Rev. Syst. Biol. Med. *2*, 336–361.

Shi, L.Z., Wang, R., Huang, G., Vogel, P., Neale, G., Green, D.R., and Chi, H. (2011). HIF1alpha-dependent glycolytic pathway orchestrates a metabolic checkpoint for the differentiation of TH17 and Treg cells. J. Exp. Med. *208*, 1367–1376.

Strickland, D.H., Stumbles, P.A., Zosky, G.R., Subrata, L.S., Thomas, J.A., Turner, D.J., Sly, P.D., and Holt, P.G. (2006). Reversal of airway hyperresponsiveness by induction of airway mucosal CD4+CD25+ regulatory T cells. J. Exp. Med. *203*, 2649–2660.

Stumbles, P.A., Thomas, J.A., Pimm, C.L., Lee, P.T., Venaille, T.J., Proksch, S., and Holt, P.G. (1998). Resting respiratory tract dendritic cells preferentially stimulate T helper cell type 2 (Th2) responses and require obligatory cytokine signals for induction of Th1 immunity. J. Exp. Med. *188*, 2019–2031.

Subramanian, A., Tamayo, P., Mootha, V.K., Mukherjee, S., Ebert, B.L., Gillette, M.A., Paulovich, A., Pomeroy, S.L., Golub, T.R., Lander, E.S., and Mesirov, J.P. (2005). Gene set enrichment analysis: a knowledge-based approach for interpreting genome-wide expression profiles. Proc. Natl. Acad. Sci. USA *102*, 15545–15550.

Sukumar, M., Liu, J., Ji, Y., Subramanian, M., Crompton, J.G., Yu, Z., Roychoudhuri, R., Palmer, D.C., Muranski, P., Karoly, E.D., et al. (2013). Inhibiting glycolytic metabolism enhances CD8+ T cell memory and antitumor function. J. Clin. Invest. *123*, 4479–4488.

Sun, C.M., Hall, J.A., Blank, R.B., Bouladoux, N., Oukka, M., Mora, J.R., and Belkaid, Y. (2007). Small intestine lamina propria dendritic cells promote de novo generation of Foxp3 T reg cells via retinoic acid. J. Exp. Med. *204*, 1775–1785.

Takeda, K., Ho, V.C., Takeda, H., Duan, L.J., Nagy, A., and Fong, G.H. (2006). Placental but not heart defects are associated with elevated hypoxia-inducible factor alpha levels in mice lacking prolyl hydroxylase domain protein 2. Mol. Cell. Biol. *26*, 8336–8346.

Trapnell, C., Roberts, A., Goff, L., Pertea, G., Kim, D., Kelley, D.R., Pimentel, H., Salzberg, S.L., Rinn, J.L., and Pachter, L. (2012). Differential gene and transcript expression analysis of RNA-seq experiments with TopHat and Cufflinks. Nat. Protoc. *7*, 562–578.

Valastyan, S., and Weinberg, R.A. (2011). Tumor metastasis: Molecular insights and evolving paradigms. Cell *147*, 275–292.

Weiss, J.M., Bilate, A.M., Gobert, M., Ding, Y., Curotto de Lafaille, M.A., Parkhurst, C.N., Xiong, H., Dolpady, J., Frey, A.B., Ruocco, M.G., et al. (2012). Neuropilin 1 is expressed on thymus-derived natural regulatory T cells, but not mucosa-generated induced Foxp3+ T reg cells. J. Exp. Med. *209*, 1723–1742.

Wikstrom, M.E., and Stumbles, P.A. (2007). Mouse respiratory tract dendritic cell subsets and the immunological fate of inhaled antigens. Immunol. Cell Biol. *85*, 182–188.

Yadav, M., Louvet, C., Davini, D., Gardner, J.M., Martinez-Llordella, M., Bailey-Bucktrout, S., Anthony, B.A., Sverdrup, F.M., Head, R., Kuster, D.J., et al. (2012). Neuropilin-1 distinguishes natural and inducible regulatory T cells among regulatory T cell subsets in vivo. J. Exp. Med. *209*, 1713–1722.

STAR★METHODS

KEY RESOURCES TABLE

REAGENT or RESOURCE	SOURCE	IDENTIFIER
Antibodies		
Anti-Mouse/Rat Foxp3 (clone FJK-16 s)	Ebioscience	Cat# 17-5773
Anti-Mouse IFN-γ (clone XMG1.2)	Ebioscience	Cat# 17-7311
Anti-Mouse/Rat IL-17A (clone eBio17B7)	Ebioscience	Cat# 25-7177
Anti-Human/Mouse T-bet (clone eBio4B10)	Ebioscience	Cat# 12-5825
Anti-Mouse ROR gamma (t) (clone B2D)	Ebioscience	Cat# 12-6981
Anti-Mouse CD304 (Neuropilin-1) (clone 3DS304M)	Ebioscience	Cat# 25-3041
Anti-Mouse TCR beta (clone H57-597)	Ebioscience	Cat# 47-5961
Anti-Mouse IL-13 (clone eBio13A)	Ebioscience	Cat# 12-7133
Anti-Mouse Granzyme B (clone NGZB)	Ebioscience	Cat# 12-8898
Anti-Mouse Perforin (clone eBioOMAK-D)	Ebioscience	Cat# 12-9392
Anti-Human Foxp3 (PCH101)	Ebioscience	Cat# 17-4776
Anti-Mouse CD45.1 (clone A20)	BD Biosciences	Cat# 558701
Anti-Mouse CD4 (clone RM4-5)	BD Biosciences	Cat# 563727
Anti-Mouse CD25 (clone PC61)	BD Biosciences	Cat# 553866
Anti-Mouse CD62L (clone MEL-14)	BD Biosciences	Cat# 553150
Anti-Mouse CD44 (clone IM7)	BD Biosciences	Cat# 559250
Anti-Mouse CD8a (clone 53-6.7)	BD Biosciences	Cat# 553035
Anti-Mouse CD152 (CTLA4) (clone UC10-4F10-11)	BD Biosciences	Cat# 553720
Anti-Mouse GITR (clone DTA-1)	BD Biosciences	Cat# 558119
Anti-Mouse IL-4 (clone 11B11)	BD Biosciences	Cat# 562044
Anti-Mouse IL-5 (clone TRFK5)	BD Biosciences	Cat# 554395
Anti-Human CD4 (clone RPA-T4)	BD Biosciences	Cat# 560158
Anti-Human CD45RO (clone UCHL1)	BD Biosciences	Cat# 562791
Anti-Human CD45RA (clone HI100)	BD Biosciences	Cat# 555489
Anti-Human CD62L (clone DREG-56)	BD Biosciences	Cat# 555544
Anti-Human CD197 (CCR7) (clone 3D12)	BD Biosciences	Cat# 560548
Anti-Mouse IgG Fab2	Cell Signaling Technology	Cat# 4410S
Mouse monoclonal HDAC1 (clone 10E2)	Cell Signaling Technology	Cat# 5356S
Mouse polyclonal HIF-1 alpha	Novus Biologicals	Cat# NB100-479
*InVivo*mAb anti-mouse IFN-γ neutralizing antibody (clone XMG1.2)	BioXCell	Cat# BE0055
*InVivo*mAb anti-mouse IL-4 neutralizing antibody (clone 11B11)	BioXcell	Cat# BE0045
Anti-Mouse CD3 Functional Grade Purified (clone 17A2)	Ebioscience	Cat# 14-0032
Anti-Mouse CD28 Functional Grade Purified (clone 37.51)	Ebioscience	Cat# 16-0281
Anti-Human CD3 Functional Grade Purified (clone OKT3)	Ebioscience	Cat# 16-0037
Anti-Human CD28 Functional Grade Purified (clone CD28.2)	Ebioscience	Cat# 16-0289
Chemicals, Peptides, and Recombinant Proteins		
α-GalCer Loaded Recombinant CD1d Tetramer	Proimmune	Cat# E001-2A
Dimethyloxalylglycine (DMOG)	Sigma-Aldrich	Cat# D3695
Rapamycin	Sigma-Aldrich	Cat# R8781

Continued

REAGENT or RESOURCE	SOURCE	IDENTIFIER
2-Deoxy-D-glucose (2-DG)	Sigma-Aldrich	Cat# D6134
2-Deoxy-2-[(7-nitro-2,1,3-benzoxadiazol-4-yl) amino]-D-glucose (2-NBDG)	Sigma-Aldrich	Cat# 72987
Recombinant Human IL-2 Protein	R&D Systems	Cat# 202-IL
Recombinant Human IL-12 Protein	R&D Systems	Cat# 219-IL
Recombinant Human IL-6 Protein	R&D Systems	Cat# 206-IL
Recombinant Human TGF-β Protein	R&D Systems	Cat# 240-B
House Dust Mite extract (*D. Pteronyssinus;* low-endotoxin)	Stallergenes Greer	Cat# B70
Taqman PCR Master Mix, no AmpErase UNG	Applied Biosystems	Cat# 4324018
Critical Commercial Assays		
RNeasy Plus Mini Kit	QIAGEN	Cat# 74134
TruSeq RNA Library Preparation Kit v2	Illumina	Cat# RS-122-2001
Mouse anti-dsDNA Ig's ELISA kit	Alpha Diagnostic	Cat# 5110
Mouse Anti-Nuclear Antigens (ANA/ENA) Ig's	Alpha Diagnostic	Cat# 5210
High-Capacity cDNA Reverse Transcription Kit with RNase Inhibitor	Applied Biosystems	Cat# 4374966
Mouse IFN gamma ELISA Ready-SET-Go	Ebioscience	Cat#
NE-PER Nuclear and Cytoplasmic Extraction Reagents	Thermo Scientific	Cat# 78833
Pierce BCA Protein Assay Kit	Thermo Scientific	Cat# 23225
Seahorse Bioassay	Agilent Technologies	Cat# 102416
Mouse Foxp3 Methylation Panel	EpigenDx	http://epigendx.com/d/products/methylation-assay-panels/foxp3-panel/
Deposited Data		
Raw data files for RNA sequencing	NCBI Gene Expression Omnibus	GEO: GSE85131
Experimental Models: Cell Lines		
Mouse: B16-F10 melanoma	ATCC	Cat# CRL-6475
Mouse: primary T lymphocytes	This paper	N/A
Human: primary healthy donor T lymphocytes	This paper	N/A
Experimental Models: Organisms/Strains		
Mouse: C57BL/6J	The Jackson Laboratory	Stock No: 000664
Mouse: B6.129S7-Rag1^{tm1Mom}/J	The Jackson Laboratory	Stock No: 002216
Mouse: B6.Cg-*Rag1*^{tm1Mom} *Tyrp1*$^{B-w}$ Tg(Tcra,Tcrb)9Rest/J	The Jackson Laboratory	Stock No: 008684
Mouse: Tg(CD4-cre)1Cwi/BfluJ	The Jackson Laboratory	Stock No: 017336
Mouse: *Egln1*$^{fl/fl}$	Takeda et al., 2006	N/A
Mouse: *Egln2*$^{fl/fl}$	Takeda et al., 2006	N/A
Mouse: *Egln3*$^{fl/fl}$	Takeda et al., 2006	N/A
Mouse: *Hif1a*$^{fl/fl}$	Ryan et al., 2000	N/A
Mouse: *Epas1*$^{fl/fl}$	Gruber et al., 2007	N/A
Software and Algorithms		
TopHat (v2.0.11)	Kim and Salzberg, 2011	https://ccb.jhu.edu/software/tophat/index.shtml
Cufflinks (v2.12.0)	Trapnell et al., 2012	http://cole-trapnelllab.github.io/cufflinks/
GSEA (v2.2.2)	Broad Institute	http://software.broadinstitute.org/gsea/index.jsp

CONTACT FOR REAGENT AND RESOURCE SHARING

Further information and requests for reagents may be directed to, and will be fulfilled by the corresponding author Nicholas P Restifo (restifo@nih.gov).

EXPERIMENTAL MODEL AND SUBJECT DETAILS

Mice

Experiments were approved by the Institutional Animal Care and Use Committees of the NCI and performed in accordance with NIH guidelines. C57BL/6J, $Rag1^{-/-}$ (B6.129S7-Rag1$^{tm1Mom/J}$), Ly5.1$^{+/+}$ (B6.SJL-Ptprc^{a}Pepc^b/BoyJ), TRP-1 (B6.Cg-$Rag1^{tm1Mom}$Tyrp1^{B-w}Tg(Tcra,Tcrb)9Rest/J), and $Cd4$-Cre (Tg(CD4-Cre)1Cwi/BfluJ) were purchased from The Jackson Laboratory. The following mice have been described: $Egln1^{fl/fl}$, $Egln2^{fl/fl}$, and $Egln3^{fl/fl}$ mice (Takeda et al., 2006), $Hif1a^{fl/fl}$ mice (Ryan et al., 2000), $Epas1^{fl/fl}$ mice (Gruber et al., 2007). Deletion of loxP-flanked genes in T cells was achieved by crossing to $Cd4$-Cre mice to obtain animals with homozygous loxP-flanked alleles without Cre or hemizygous for Cre. All mice were previously backcrossed over ten generations to the C57BL/6 background. For all in vivo studies (experimental metastasis, house dust mite challenge) age and sex matched WT and PHD-tKO mice were used with at least 5 mice per genotype.

METHOD DETAILS

In Vitro T Cell Differentiation

CD4$^+$ T cells from spleens and lymph nodes of 6–12-week-old mice were purified by negative magnetic selection (Miltenyi) followed by sorting of naive CD4$^+$ CD62L$^+$ CD44$^-$ CD25$^-$ cells using a FACSAria II sorter (BD). Naive CD4$^+$ T cells were activated with plate-bound anti-CD3 and soluble anti-CD28 (5 μg ml^{-1} each; eBioscience) in media for 72h either under: Th0 conditions (media alone); Th1 conditions (IL-12 (10 ng ml^{-1}, R&D Systems), anti-IL-4 neutralizing antibodies (10 μg ml^{-1}); Th17 conditions (IL-6 (20 ng ml^{-1}, R&D Systems), human TGF-β1 (0.2 ng ml^{-1}, R&D Systems), anti-IFN-γ neutralizing antibodies (10 μg ml^{-1}) and anti-IL-4 neutralizing antibodies (10 μg ml^{-1}); or iT$_{reg}$ conditions (human TGF-β1 (0-2 ng ml^{-1}, as indicated)). For human in vitro iT$_{reg}$ induction assays, naive CD4$^+$CD45RA$^+$CD45RO$^-$CD62L$^+$CCR7$^+$ cells were FACS purified from three biologically independent healthy donor buffy coats and activated with plate-bound human anti-CD3 and soluble anti-CD28 (5 μg ml^{-1} each; eBioscience) with human TGF-β1 (5 ng mL^{-1}, R&D Systems) and recombinant human IL-2 (20 CU). Mouse and human cells were cultured under standard incubator conditions or 5% or 2% oxygen as indicated (Thermo Scientific-Hera Cell incubator equipped to replace oxygen with nitrogen) through the entire duration of culture. Where indicated, the PHD protein inhibitor DMOG (0.5 – 1.0 mM, Sigma-Aldrich), Rapamycin (50 nM, Sigma-Aldrich), or 2-deoxyglucose (1 μM, Sigma-Aldrich) was added for the duration of in vitro culture.

Histopathology

Lungs were isolated from WT and PHD-tKO mice and fixed in 10% formalin, embedded in methylacrylate, sectioned, and H&E stained. Sections were blindly evaluated by a veterinary pathologist. The presence of chronic, active inflammation, vasculitis, and hemorrhage in the alveoli was quantified on a standardized severity score system (0 least severe, 3 most severe).

House Dust Mite Airway Challenge

WT and PHD-tKO mice were sensitized with 25 μg of house dust mite (HDM, *D. Pteronyssinus*; low-endotoxin, Greer) delivered to the retropharyngeal space in sterile PBS on days 0, 1 and 2. Animals were challenged with 5 μg of HDM on days 15, 16, 17 and 18, and euthanized on day 19.

Antibodies and Flow Cytometry

The following fluorescent dye-conjugated antibodies against surface and intracellular antigens were used: anti-FOXP3 (FJK-16 s), anti-IL-17A (eBio17B7), anti-IFN-γ (XMG1.2), anti-Tbet (eBio4B10), anti-Ror gamma (t) (B2D), anti-CD304 (Nrp-1, 3DS304M), anti-mouse TCR-beta (H57-597), anti-IL-13 (eBio13A), anti-Granzyme B (NGZB), and anti-Perforin (eBioOMAK-D) (eBioscience); anti-CD45.1 (A20), anti-CD4 (RM4-5), anti-CD25 (PC61), anti-CD62L (MEL-14), anti-CD44 (IM7), anti-CD8a (53-6.7), anti-CD152 (CTLA4, UC10-4F10-11), anti-GITR (DTA-1), anti-IL-4 (11B11), anti-IL-5 (TRFK5) (BD Biosciences); Anti-mouse IgG Fab2 (Cell Signaling); Anti-mouse HIF1α (Abcam). For the identification of NKT cells, α-galactosyl ceramide loaded, PE-conjugated recombinant CD1d tetramers were used (Proimmune). Cells were incubated with specific antibodies for 30 min on ice in the presence of 2.4G2 monoclonal antibody to block FcγR binding. All samples were acquired with a Fortessa or LSR flow cytometer (Becton Dickinson) and analyzed using FlowJo software (TreeStar). Intranuclear staining was carried out using the FOXP3 staining kit (eBioscience). To determine cytokine expression, cellular suspensions containing T cells were stimulated in media containing phorbol 12-myristate 13-acetate, ionomycin and brefeldin-A (Leukocyte activation cocktail with Golgiplug; BD biosciences) for 4 h. After stimulation, cells were stained an amine-reactive exclusion-based viability dye (Invitrogen) and with antibodies against cell-surface antigens, fixed and permeabilized followed by intracellular staining with specific anti-cytokine antibodies. Single-cell suspensions from lung tissues were prepared by mechanical disruption (GentleMACS, Miltenyi). Countbright beads were spiked-in for the flow cytometric quantification of absolute cell number (Invitrogen).

RNA Sequencing and Analysis

All RNA-Seq analyses were performed using $\geq$ 2 biological replicates. Raw data from replicate measurements are publically available from the GEO repository. Total RNA was prepared from cells using the RNeasy Plus Mini kit (QIAGEN). 200 ng of total RNA was

subsequently used to prepare RNA-Seq library by using TruSeq RNA sample prep kit (Illumina) according to manufacturer's instructions. Paired-end RNA sequencing was performed on a HiSeq 2000 (Illumina). Sequenced reads were aligned to the mouse genome (NCBI37/mm9) with Tophat 2.0.11(Kim and Salzberg, 2011) and uniquely mapped reads were used to calculate gene expression. RefSeq gene database (mm9) was downloaded from the UCSC genome browser for RNA-Seq analysis. RNA-Seq reads were mapped to mm9 (UCSC) using Bowtie. Gene expression of annotated transcripts was calculated from mapped RNA-Seq reads using Cuffdiff to obtain RPKM-normalized gene expression values (Trapnell et al., 2012). Two-tailed t tests were performed to identify differentially expressed genes after applying the Benjamini-Hochberg correction for multiple testing. Gene set enrichment analysis was performed as previously described (Subramanian et al., 2005).

Autoantibody Enzyme-Linked Immunosorbent Assay
For measurement of antinuclear (ANA) and anti-dsDNA autoantibodies, ELISA assays were performed on mouse serum according to manufacturer's instructions (Alpha Diagnostic International). ELISA quantification of IFN-γ in cell supernatants collected after 72h or stimulation was performed according to manufacturer's instructions (Ebioscience).

Quantitative Reverse-Transcription Polymerase Chain Reaction
Cells were sorted or transferred into RNALater solution (Ambion) and stored at $-80\,°C$. Total RNA from pelleted cells was isolated using the RNeasy Plus mini kit (QIAGEN). First-strand cDNA synthesis was performed using random priming with the high-capacity cDNA synthesis kit (Applied Biosystems) in the presence of SuperaseIn RNase inhibitor (Ambion). cDNA was used as a template for quantitative PCR reactions using Taqman primer-probes against specified mRNA transcripts (Applied Biosystems). Reactions were performed using Universal PCR Mastermix (Applied Biosystems). FAM channel intensity were normalized to ROX intensity, and C_t values were calculated using automatically determined threshold values using SDS software (Applied Biosystems).

Immunoblot Analysis
Nuclear extracts were isolated (NE-PER kit; Pierce) and $\sim15\,\mu g$ protein was loaded in each lane of a mini-protean precast TGX gel (Biorad). Protein was transferred onto activated PVDF membrane (Biorad), blocked with 5% BSA in TBST at RT for 1h, and incubated in 1° antibody at 4°C overnight. HIF1α (NB100-449, Novus) and loading control HDAC1 (10E2, Cell Signaling Technology) antibodies were used at 1:1000 dilution in TBST. Samples were washed 5x with TBST, incubated with 2° antibody at 1:5000 dilution in TBST for 2h, and washed 5x with TBST. Protein was visualized with enhanced chemiluminescence (ThermoScientific) and autoradiography film. Densitometry was calculated using ImageJ software.

Bone Marrow Chimeras
For bone marrow reconstitution experiments, $Rag1^{-/-}$ mice were administered 1,000 Gy total-bodγ-radiation from a ^{137}Cs source before intravenous injection of BM cells depleted of mature lineages from single-cell bone-marrow preparations using antibody-coupled magnetic beads (Miltenyi). Bone marrow from 6–10-week-old donor mice were used.

In Vivo iT$_{reg}$ Induction
$Rag1^{-/-}$ mice were injected intravenously with 4×10^5 CD4$^+$ CD25$^-$ CD45RB^{high} cells from wild-type or PHD-tKO mice. On day 21 to 23, transferred cells were isolated and analyzed for FoxP3 expression by flow cytometry.

In Vivo T$_{reg}$ Stability
$Rag1^{-/-}$ mice were injected intravenously with 4×10^5 CD4$^+$ CD25$^+$ cells from wild-type or PHD-tKO mice. On day 7, transferred cells were isolated and analyzed for FoxP3 expression by flow cytometry.

In Vitro T$_{reg}$ Stability
CD4$^+$ CD25$^+$ T$_{reg}$ cells were FACS purified from wild-type or PHD-tKO mice and stimulated in vitro with anti-CD3 (1 μg mL^{-1}) in the presence of IL-2 (100 IU). Foxp3 expression was analyzed by flow cytometry 72h post-stimulation.

In Vitro Suppression Assay
Naive CD4$^+$ T cells were FACS purified from Foxp3-GFP mice and stimulated in vitro in the presence of TGF-β ± DMOG for 72h. Foxp3-GFP$^+$ iT$_{reg}$ cells were then FACS purified from VEH and DMOG treated cultures. VEH and DMOG iT$_{reg}$ cells were cultured in 96-well round-bottom plates with 5×10^4 CFSE-labeled naive CD45.1 CD4$^+$ CD25$^-$ (T$_{resp}$) cells along with 1×10^4 CD11c$^+$ dendritic cells used as antigen-presenting cells, isolated by immunomagnetic selection (Miltenyi). Cells were stimulated with anti-CD3 antibody (1 μg mL^{-1}, BD Biosciences) for 72h at 37 and 5% CO_2. T$_{resp}$ cell proliferation was measured by CFSE dilution by flow cytometry.

Extracellular Acidification Rate and Glucose Uptake
Extracellular acidification rates (ECAR) and oxygen consumption rates (OCR) were measured at 37°C using an XF24 extracellular analyzer (Seahorse Bioscience). ECAR was measured in XF media (nonbuffered RPMI 1640 containing 25 mM glucose, 2 mM

L-glutamine, and 1 mM sodium pyruvate) under basal conditions. To determine glucose uptake, T cells were incubated with 100 μM 2-NBDG (Invitrogen) for 2 hr before measuring fluorescence by flow cytometry.

Foxp3 TSDR Methylation

500 ng of sample DNA from WT and PHD-tKO FACS purified CD4+ CD25+ Treg and CD4+ CD25- non-Treg cells was bisulfite treated (Epigendx) and column purified (Zymogen). PCR amplification of the Foxp3 TSDR locus region (nucleotides −2369 to −2207 relative to Foxp3 start codon) was performed using biotinylated PCR primer (Epigendx). PCR products were bound to Streptavidin Sepharose HP (GE Healthcare Life Sciences), washed, and denatured with NaOH. Pyrosequencing primer was annealed to the purified single-stranded PCR product and sequencing was performed using the Pyrosequencing PSQ96 HS System according to manufacturer's instructions (Pyrosequencing, QIAGEN). The methylation status of each locus was analyzed individually as a T/C SNP using QCpG software (Pyrosequencing, QIAGEN).

Experimental Metastasis

B16F10 (B16) melanoma cell line was obtained from the NCI tumor repository and passaged in Dulbecco's Modified Eagle Medium (Invitrogen) supplemented with 10% fetal calf serum. 2.5×10^5 B16 cells were injected subcutaneously in flanks and intravenously through the tail vein. Tumor implantation experiments were performed in littermate mice of 8-12 weeks of age. Subcutaneous tumors were measured at serial time points following implantation using digital calipers and the tumor area was calculated as the product of perpendicular diameter. Lung tumor nodules were enumerated by gross count of visible sites of disease. Micrometastatic lesions were quantified following H&E stain of lung sections, and sections consistent with melanoma histology were circumscribed by a certified veterinarian. All subcutaneous and pulmonary tumor measurements were performed in a blinded manner. IFN-γ depletion was performed using intraperitoneal injection of 250 μg anti-IFN-γ (XMG1.2, BioXcell) at indicated time points.

Adoptive Cell Transfer

Mice 6 to 12 weeks of age (n = 6-10 for all groups) were injected intravenously or subcutaneously with 2.5×10^5 B16 melanoma cells. 5-10 days later mice were treated with adoptively transferred TRP-1 specific CD4+ T cells derived from TCR transgenic splenocytes and stimulated in vitro in the presence or absence of the PHD inhibitor DMOG. At the time of ACT mice received 500 Gy total body irradiation.

QUANTIFICATION AND STATISTICAL ANALYSIS

Statistical parameters including the exact value of n, the definition of center, dispersion and precision measures (mean ± SEM) and statistical significance are reported in the Figures and Figure Legends. Data is judged to be statistically significant when $p < 0.05$ by two-tailed Student's t test. In figures, asterisks denote statistical significance as calculated by Student's t test (*, $p < 0.05$; **, $p < 0.01$; ***, $p < 0.001$; ****, $p < 0.0001$). Survival significance in adoptive cell transfer studies was determined by a Log-rank Mantel-Cox test. Statistical analysis was performed in GraphPad PRISM 6.

DATA AND SOFTWARE AVAILABILITY

Data Resources

Raw data files for the RNA sequencing analysis have been deposited in the NCBI Gene Expression Omnibus under accession number GEO: GSE85131.
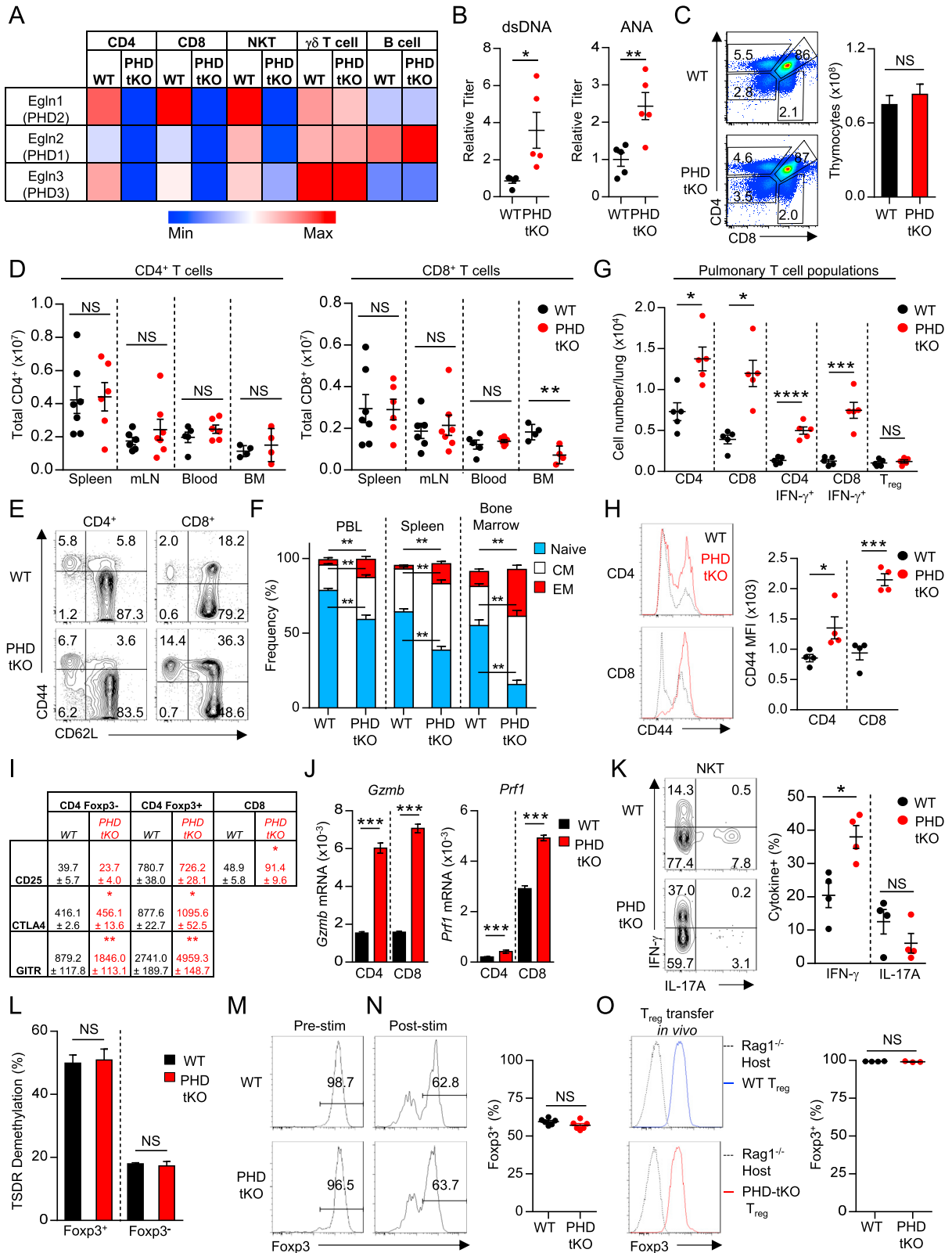
Figure S1. PHD Proteins Function within T Cells to Suppress Spontaneous Pulmonary Inflammation, Related to Figure 1

(A) Expression of *Egln1* (PHD2), *Egln2* (PHD1), and *Egln3* (PHD3) mRNA transcripts in $CD4^+$ and $CD8^+$ T cells, NKT cells, $\gamma\delta$-T cells and B cells FACS purified from the spleens of littermate matched $Egln1^{fl/fl}$ $Egln2^{fl/fl}$ $Egln3^{fl/fl}$ $CD4Cre^{-/-}$ (WT) or $Egln1^{fl/fl}$ $Egln2^{fl/fl}$ $Egln3^{fl/fl}$ $CD4Cre^{+/-}$ (PHD-tKO) mice. Expression of each transcript is normalized to *Actb*. Heatmap is row normalized to minimum and maximum value for each *Egln* transcript across indicated cell type and mouse genotype.

(B) Titer of anti-dsDNA and anti-nuclear antibodies (ANA) in the sera of WT and PHD-tKO animals. Relative titer normalized to average WT levels.

(C) Phenotypic distribution and total thymocyte count in the thymus of WT and PHD-tKO mice as assessed by flow cytometry.

(D) Total number of $CD4^+$ and $CD8^+$ T lymphocytes in the spleen, mesenteric lymph nodes (mLN), blood, and bone marrow (BM) from WT or PHD-tKO mice.

(E) Representative flow cytometry demonstrating steady state expression of markers of T cell differentiation CD44 and CD62L in $CD4^+$ and $CD8^+$ T cells in the peripheral blood of WT and PHD-tKO mice.

(F) Differentiation state (Naive, CM, EM) of $CD8^+$ T cells in the peripheral blood, spleen, and bone marrow of WT and PHD-tKO mice as determined by flow cytometry expression of CD44 and CD62L.

(G) Total numbers of the indicated pulmonary T cell populations in the lungs of WT and PHD-tKO mice.

(H) CD44 expression on pulmonary $CD4^+$ and $CD8^+$ T cells from WT and PHD-tKO mice. Representative flow cytometry histograms and replicate values are shown.

(I) Mean fluorescence intensity (MFI) of T cell activation markers CD25, CTLA-4, and GITR, as determined by flow cytometry, expressed on pulmonary $CD4^+$ $Foxp3^-$, $CD4^+$ $Foxp3^+$, and $CD8^+$ T cells from WT and PHD-tKO mice. Average MFI $\pm$ SEM are reported in the table. * indicates significant increase in expression in PHD-tKO mice compared to WT for each indicated marker and cell type.

(J) Expression of cytolytic effector molecules Granzyme B (*Gzmb*) and Perforin (*Prf1*) in pulmonary $CD4^+$ and $CD8^+$ T cells purified from WT and PHD-tKO mice. Gene expression is normalized to *Actb*.

(K) Pulmonary NKT cell expression of effector cytokines IFN-γ and IL-17A in WT and PHD-tKO mice. Representative flow cytometry and replicate values are shown.

(L) Methylation status of CpG motifs of the TSDR region of the *Foxp3* locus (CpG sites between -2369 to -2207 from *Foxp3* start codon) in $Foxp3^+$ and $Foxp3^-$ $CD4^+$ T cells isolated from the spleen of WT and PHD-tKO mice.

(M) Foxp3 expression in $CD4^+$ $CD25^+$ T cells FACS purified from WT and PHD-tKO mice.

(N) Foxp3 expression in $CD4^+$ $CD25^+$ T cells FACS purified from WT and PHD-tKO mice and stimulated in vitro for 72h.

(O) Foxp3 expression in CD4+ CD25+ T cells FACS purified from WT and PHD-tKO mice one week following injection into $Rag1^{-/-}$ host mice. $Rag1^{-/-}$ splenocytes were used to determine Foxp3-negative gate. Representative flow cytometry and replicate values are shown.

Dots represent individual mice. Data are representative of ≥ 2 independent experiments with ≥ 3 mice per group. Bars and error represent mean $\pm$ SEM of replicate measurements. *p < 0.05, **p < 0.01, ***p < 0.001, ****p < 0.0001 (Student's t test).

A

B
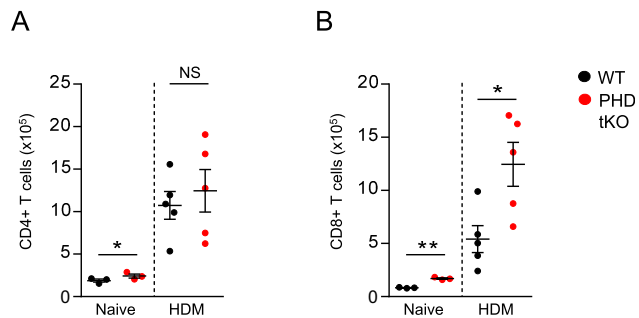
Figure S2. T-Cell-Intrinsic PHD Proteins Restrain Th1 Inflammation against Innocuous Antigens, Related to Figure 2

(A and B) Total number of CD4+ (A) and CD8+ (B) T cells in the lungs of WT and PHD-tKO mice following sensitization and challenge with HDM extract.

A

DMOG/Veh Log$_2$(FC)

Gata3
Ifng
Tbx21
Foxp3 *Rorc*

p<0.01

B

PHD-tKO/WT UP

NES: 4.18
P-value < 0.0001

Zero cross at 1315

'na_pos' (positively correlated)
'na_neg' (negatively correlated)

Rank in Ordered Dataset

C

D

WT
PHD-tKO
PHD-tKO + anti-IFN-γ

Foxp3$^+$ Gated

E

Foxp3-GFP

F

No T$_{reg}$

1:1
T$_{eff}$:T$_{reg}$

78.5

56.1
58.6

VEH T$_{reg}$
DMOG T$_{reg}$

CFSE

No T$_{reg}$
Veh T$_{reg}$
DMOG T$_{reg}$

G

LP   Lung

WT

PHD tKO

19.6   5.9

14.2   6.8

CD4
IL-17A

WT
PHD tKO

NS
NS

H

WT

PHD tKO

70.2   10.3
19.4   0.0

72.5   8.9
18.5   0.0

RORγt
IL-17A

NS

NS

I

WT

PHD tKO

22.6   69.1
1.5   6.8

38.8   56.3
1.2   3.7

CD44
CD62L

WT
PHD tKO

NS

SCM   CM   EM

J

WT
PHD tKO

Granzyme B

Perforin

WT   PHD tKO

(legend on next page)

Figure S3. PHD Proteins Regulate Reciprocal iT$_{reg}$ and Th1 Differentiation Programs, Related to Figure 3

(A) Volcano plot of all expressed transcripts (RPKM $\geq$ 1) determined by RNA-seq analysis of CD4$^+$ T cells stimulated in vitro (anti-CD3, anti-CD28 5 μg mL^{-1} each, TGF-β 2.0 ng mL^{-1}) in the presence or absence of DMOG (1mM). Transcripts significantly (p < 0.01) overexpressed (FC $\geq$ 2, red) and under-expressed (FC $\leq$ 0.5, blue) in DMOG treated cells are highlighted.

(B) Geneset enrichment analysis with a gene-set composed of all significantly overexpressed transcripts in PHD-tKO versus WT CD4$^+$ T cells in T cells stimulated in the presence of DMOG compared to Vehicle. Transcripts overexpressed in the presence of DMOG significantly enrich with transcripts overexpressed in PHD-tKO cells compared to WT. GSEA significance was tested using a weighted Kolmogorov-Smirnov test.

(C) In vivo iT$_{reg}$ cell conversion of naive WT and PHD-tKO CD4$^+$ T cells. Foxp3 was assessed by flow cytometry, replicate values are shown.

(D) T-bet expression in Foxp3$^+$ iT$_{reg}$ cells generated from WT and PHD-tKO CD4$^+$ T cells stimulated in the presence of TGF-β (0.2 ng mL^{-1}) $\pm$ the addition of IFN-γ blocking antibodies (XMG1.2). T-bet MFI determined by flow cytometry, replicate values are shown.

(E) Gating strategy to isolate Foxp3-GFP$^+$ iT$_{reg}$ cells derived from naive CD4$^+$ T cells purified from Foxp3-GFP mice and stimulated in vitro in the presence of TGF-β $\pm$ DMOG (0.5mM).

(F) Suppressive capacity of Foxp3-GFP$^+$ iT$_{reg}$ cells derived in the absence (VEH T$_{reg}$) or presence of DMOG (DMOG T$_{reg}$) (as described in (E). VEH T$_{reg}$ and DMOG T$_{reg}$ were mixed with CFSE labeled naive CD4$^+$ CD45.1$^+$ responder cells, soluble CD3 (1 μg/mL), and CD11c$^+$ cells purified by magnetic bead isolation. Proliferation of responder cells was determined by CFSE dilution. Representative flow cytometry and replicate values are shown.
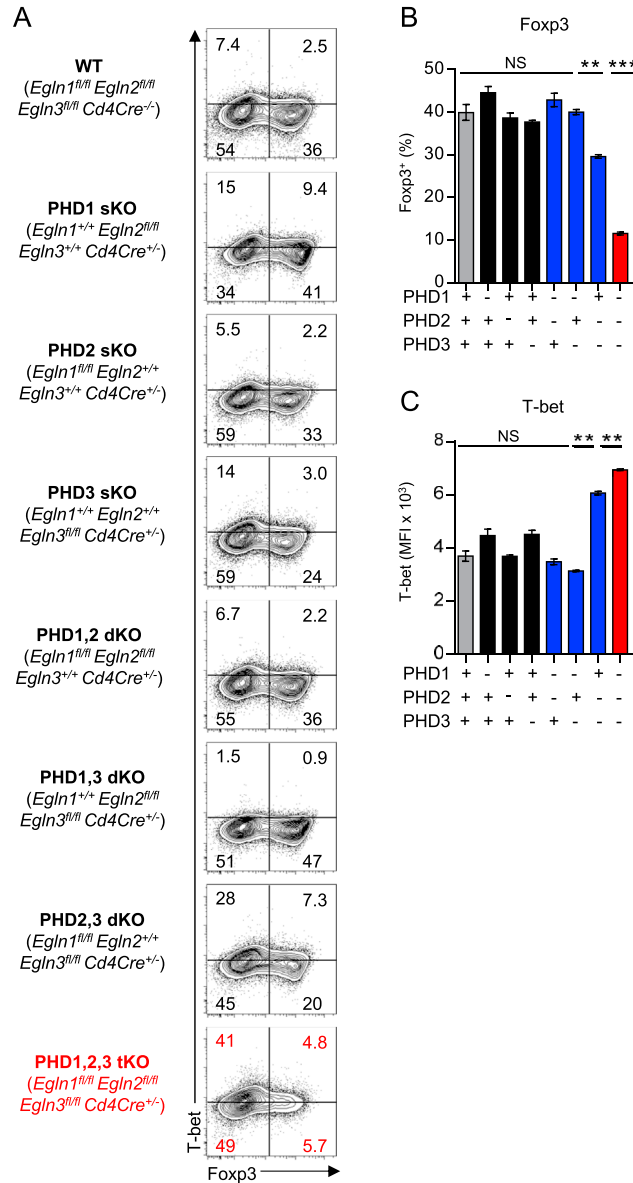
(G) IL-17A production from small intestine lamina propria and lung CD4$^+$ T cells isolated from WT and PHD-tKO mice and stimulated briefly ex vivo. Representative flow cytometry and replicate values are shown.

(H) IL-17A and RORγt expression in CD4$^+$ T cells isolated from WT and PHD-tKO mice and stimulated in vitro under established Th17 polarizing conditions (anti-CD3, anti-CD28 5 μg mL^{-1} each, TGF-β 0.2ng mL^{-1}, IL-6 20ng mL^{-1}, anti-IFN-γ 10 μg mL^{-1}, anti-IL4 10 μg mL^{-1}). Representative flow cytometry and replicate values for IL-17A$^+$ percentage and RORγt MFI are shown.

(I) CD44 and CD62L expression in CD8$^+$ T cells isolated from WT and PHD-tKO mice and stimulated in vitro (anti-CD3, anti-CD28 1 μg mL^{-1} each, IL-2 100 IU) for 48 hr. Cells were removed from stimulation and expanded in the presence of IL-2 for an additional 72h. Representative flow cytometry and replicate values are shown. SCM: CD44$^-$ CD62L$^+$, CM: CD44$^+$ CD62L$^+$, EM: CD44$^+$ CD62L$^-$

(J) Intracellular expression of cytolytic molecules Granzyme B and Perforin in WT and PHD-tKO CD8$^+$ T cells stimulated as described in (I).

Data are representative of $\geq$ 2 independent experiments with $\geq$ 3 mice per group. Bars and error represent mean $\pm$ SEM of replicate measurements. *p < 0.05, **p < 0.01, ****p < 0.0001 (Student's t test).

A

WT
(*Egln1$^{fl/fl}$ Egln2$^{fl/fl}$*
Egln3$^{fl/fl}$ Cd4Cre$^{-/-}$)

| 7.4 | 2.5 |
| 54 | 36 |

PHD1 sKO
(*Egln1$^{+/+}$ Egln2$^{fl/fl}$*
Egln3$^{+/+}$ Cd4Cre$^{+/-}$)

| 15 | 9.4 |
| 34 | 41 |

PHD2 sKO
(*Egln1$^{fl/fl}$ Egln2$^{+/+}$*
Egln3$^{+/+}$ Cd4Cre$^{+/-}$)

| 5.5 | 2.2 |
| 59 | 33 |

PHD3 sKO
(*Egln1$^{+/+}$ Egln2$^{+/+}$*
Egln3$^{fl/fl}$ Cd4Cre$^{+/-}$)

| 14 | 3.0 |
| 59 | 24 |

PHD1,2 dKO
(*Egln1$^{fl/fl}$ Egln2$^{fl/fl}$*
Egln3$^{+/+}$ Cd4Cre$^{+/-}$)

| 6.7 | 2.2 |
| 55 | 36 |

PHD1,3 dKO
(*Egln1$^{+/+}$ Egln2$^{fl/fl}$*
Egln3$^{fl/fl}$ Cd4Cre$^{+/-}$)

| 1.5 | 0.9 |
| 51 | 47 |

PHD2,3 dKO
(*Egln1$^{fl/fl}$ Egln2$^{+/+}$*
Egln3$^{fl/fl}$ Cd4Cre$^{+/-}$)

| 28 | 7.3 |
| 45 | 20 |

PHD1,2,3 tKO
(*Egln1$^{fl/fl}$ Egln2$^{fl/fl}$*
Egln3$^{fl/fl}$ Cd4Cre$^{+/-}$)

| 41 | 4.8 |
| 49 | 5.7 |

T-bet → Foxp3

B

Foxp3

NS   **   ***

Foxp3$^+$ (%)

PHD1	+	-	+	+	-	-	+	-
PHD2	+	+	-	+	-	+	-	-
PHD3	+	+	+	-	+	-	-	-

C

T-bet

NS   **   **

T-bet (MFI x 10^3)

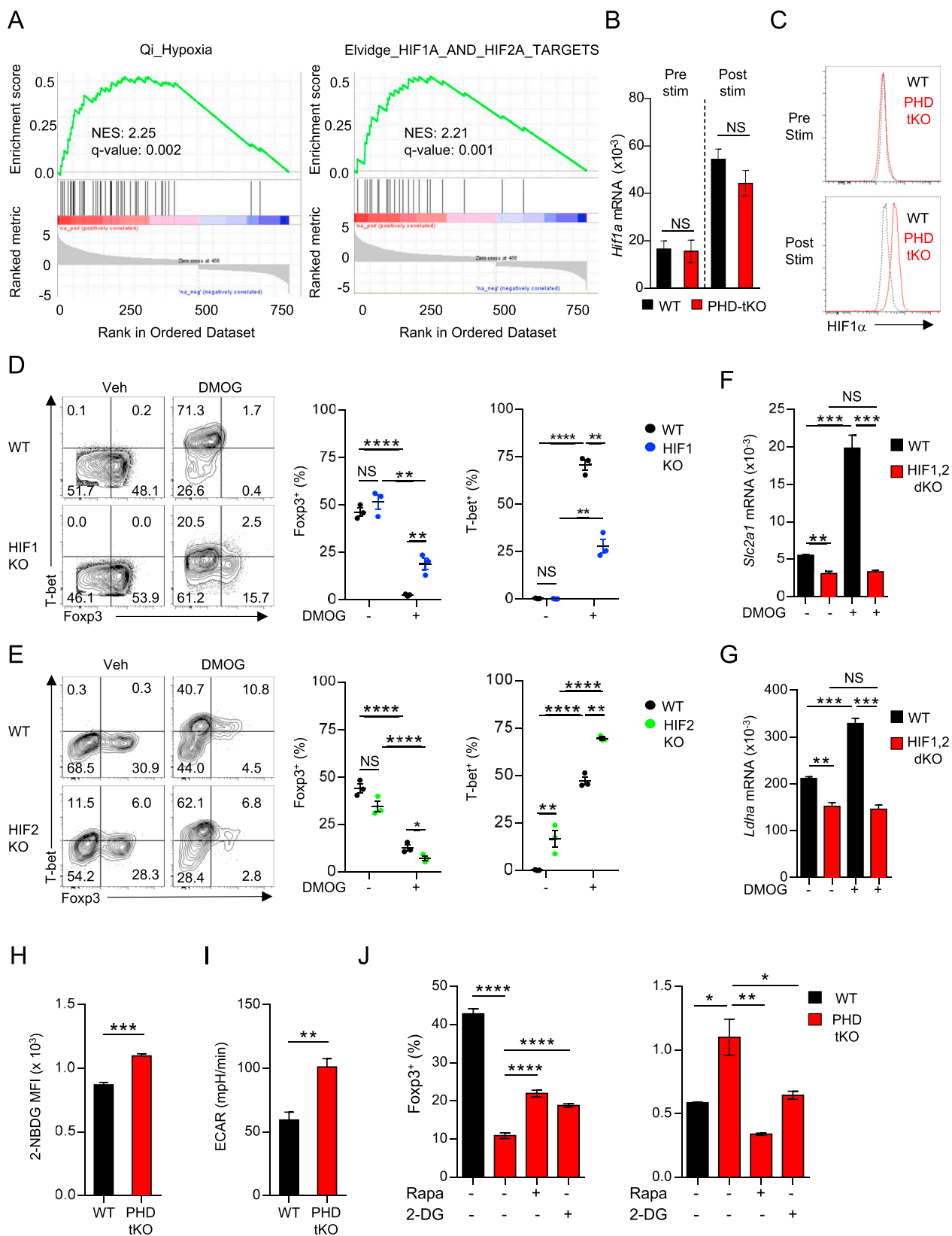| PHD1 | + | - | + | + | - | - | + | - |
| PHD2 | + | + | - | + | - | + | - | - |
| PHD3 | + | + | + | - | + | - | - | - |

Figure S4. PHD Proteins Are Functionally Redundant in T Lymphocytes, Related to Figures 4A–4C

Flow cytometry of Foxp3 and T-bet expression in CD4$^+$ T cells isolated from the indicated PHD knockout genotype and stimulated in vitro in the presence of TGF-β (0.2 ng mL^{-1}) for 72h.

(A–C) Representative flow cytometry (A) and replicate values for Foxp3 (B) and T-bet (C) are shown.

Data are representative of $\geq$ 2 independent experiments with $\geq$ 3 mice per group. Bars and error represent mean $\pm$ SEM of replicate measurements. *p < 0.05, **p < 0.01, ***p < 0.001 (Student's t test).

A

Qi_Hypoxia

NES: 2.25
q-value: 0.002

Elvidge_HIF1A_AND_HIF2A_TARGETS

NES: 2.21
q-value: 0.001

B

C

D

E

F

G

H

I

J

Figure S5. PHD Proteins Coordinate T Cell Specification through Repression of HIF1α and HIF2α, Related to Figure 5

(A) Gene set enrichment analysis with indicated gene sets in PHD-tKO compared with WT CD4$^+$ T cells stimulated in vitro (anti-CD3, anti-CD28 5 µg ml^{-1}, TGF-β 0.2 ng ml^{-1}). Non-random distribution of genes comprising Qi_Hypoxia and Elvidge_HIF1A_AND_HIF2A_TARGETS in PHD-tKO compared to WT cells. NES = normalized enrichment score. Significance was tested using a weighted Kolmogorov-Smirnov test.

(B) *Hif1a* mRNA expression in WT and PHD-tKO naive CD4$^+$ T cells freshly isolated ex vivo (Pre-stim) or 24h following in vitro stimulation (Post-stim).

(C) HIF1α protein expression as determined by flow cytometry in WT and PHD-tKO naive CD4$^+$ T cells freshly isolated ex vivo (Pre-stim) or 24h following in vitro stimulation (Post-stim).

(D) Foxp3 and T-bet expression in CD4$^+$ T cells isolated from WT and HIF1α KO mice and stimulated in vitro in the presence of TGF-β (0.2 ng mL^{-1}) ± DMOG (1mM) for 72h.. Representative flow cytometry and replicate values are shown. Dots represent individual mice.

(E) Foxp3 and T-bet expression in CD4$^+$ T cells isolated from WT and HIF2α KO mice and stimulated in vitro in the presence of TGF-β (0.2 ng mL^{-1}) ± DMOG (1mM) for 72h.. Representative flow cytometry and replicate values are shown. Dots represent individual mice.

(F and G) Expression of genes involved in glycolysis *Slc2a1* (F) and *Ldha* (G) in WT and HIF1,2 dKO CD4$^+$ T cells stimulated in vitro in the presence of TGF-β (0.2 ng mL^{-1}) ± DMOG (1mM) for 72h.

(H) 2-NBDG uptake in WT and PHD-tKO CD4$^+$ T cells stimulated as described in (A). Representative flow cytometry and replicate values are shown.

(I) Extracellular acidification rate (ECAR) as determined by Seahorse bioassay in CD8$^+$ T cells isolated from WT and PHD-tKO mice. Cells were stimulated in vitro for 48h and were removed from stimulation and rested for 24h prior to Seahorse analysis.

(J) Replicate measurements of Foxp3 and T-bet expression in WT and PHD-tKO CD4$^+$ T cells stimulated in vitro in the presence of TGF-β (0.2 ng mL^{-1}) with or without the addition of inhibitors of glycolytic metabolism rapamycin (Rapa) and 2-deoxyglucse (2DG).

Data are representative of ≥ 2 independent experiments with ≥ 3 mice per group. Bars and error represent mean ± SEM of replicate measurements. *p < 0.05, **p < 0.01, ***p < 0.001, ****p < 0.0001 (Student's t test).
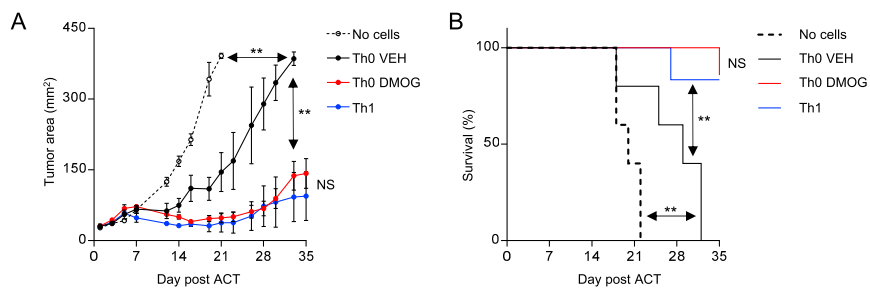
Figure S6. Inhibition of PHD Proteins Improves Adoptive Cell Transfer Immunotherapy, Related to Figure 7

(A) Subcutaneous tumor growth in mice receiving ACT of indicated cells. Adoptively transferred cells were expanded ex vivo under non-polarizing conditions ± DMOG (1mM) or Th1 specifying conditions (IL-12 10ng mL^{-1}, anti-IL-4 10 μg mL^{-1})

(B) Overall survival of tumor bearing mice treated as described in (A). Survival significance was assessed by a Log-rank Mantel-Cox test.

Data are representative of $\geq$ 2 independent experiments with > 5 mice per group. Bars and error represent mean ± SEM of replicate measurements. **p < 0.01.